AD-A068 120 ILLINOIS UNIV AT URBANA-CHAMPAIGN DEPT OF METALLURGY --ETC F/G 11/6
STRUCTURE AND DEFORMATION CHARACTERISTICS OF RHEOCAST METALS.(U)
JAN 79 R MEHRABIAN, J A SEKHAR, C Y CHEN DAAG46-76-C-0046
UNCLASSIFIED AMMRC-TR-79-2 NL

1 OF 1
AD A 068120

END
DATE FILMED
4-81
DTIC

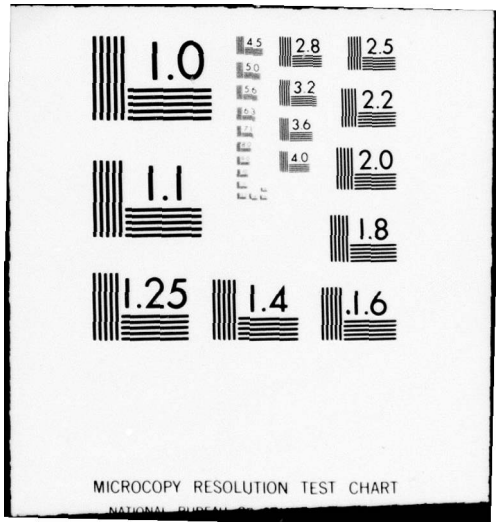
1.0
1.1
1.25
1.4
1.6
1.8
2.0
2.2
2.5
2.8
3.2
3.6
4.0
4.5
5.0
5.6
MICROCOPY RESOLUTION TEST CHART

AMMRC TR 79-2

STRUCTURE AND DEFORMATION CHARACTERISTICS OF RHEOCAST METALS

January 1979

R. Mehrabian, J. A. Sekhar, C. Y. Chen, G. J. Abbaschian,
D. G. Backman, A. Munitz, R. Wunderlin

Department of Metallurgy and Mining Engineering
Department of Mechanical and Industrial Engineering
University of Illinois at Urbana-Champaign
Urbana, IL 61801

INTERIM REPORT DAAG46-76-C-0046

ARMY MATERIALS AND MECHANICS RESEARCH CENTER
Watertown, Massachusetts 02172

The findings in this report are not to be construed as an official Department of the Army position, unless so designated by other authorized documents.

Mention of any trade names or manufacturers in this report shall not be construed as advertising nor as an official indorsement or approval of such products or companies by the United States Government.

DISPOSITION INSTRUCTIONS

Destroy this report when it is no longer needed.
Do not return it to the originator.

UNCLASSIFIED

SECURITY CLASSIFICATION OF THIS PAGE (When Data Entered)

(19) REPORT DOCUMENTATION PAGE

READ INSTRUCTIONS BEFORE COMPLETING FORM

1. REPORT NUMBER: (18) AMMRC TR-79-2

2. GOVT ACCESSION NO.

3. RECIPIENT'S CATALOG NUMBER: (9)

4. TITLE (and Subtitle): STRUCTURE AND DEFORMATION CHARACTERISTICS OF RHEOCAST METALS.

5. TYPE OF REPORT & PERIOD COVERED: Interim Report. 24 June 77 - 23 June 78,

6. PERFORMING ORG. REPORT NUMBER

7. AUTHOR(s): R. Mehrabian, J. A. Sekhar, C. Y. Chen, G. J. Abbaschian D. G. Backman, A. Munitz, R. Wunderlin

8. CONTRACT OR GRANT NUMBER(s): (15) DAAG46-76-C-0046

9. PERFORMING ORGANIZATION NAME AND ADDRESS: (16) Department of Metallurgy and Mining Engr. and Department of Mech. and Ind. Engineering University of Illinois, Urbana, IL 61801

10. PROGRAM ELEMENT, PROJECT, TASK AREA & WORK UNIT NUMBERS: D/A Project: 1L162105AH84 AMCMS Code: 62105A Agency Accession:

11. CONTROLLING OFFICE NAME AND ADDRESS: (11) Army Materials and Mechanics Research Center Watertown, Massachusetts 02172

12. REPORT DATE: Jan[redacted]79

13. NUMBER OF PAGES

14. MONITORING AGENCY NAME & ADDRESS (if different from Controlling Office)

15. SECURITY CLASS. (of this report): Unclassified

15a. DECLASSIFICATION/DOWNGRADING SCHEDULE

16. DISTRIBUTION STATEMENT (of this Report)

Approved for public release; distribution unlimited.

17. DISTRIBUTION STATEMENT (of the abstract entered in Block 20, if different from Report)

18. SUPPLEMENTARY NOTES

19. KEY WORDS (Continue on reverse side if necessary and identify by block number)

Rheocasting
Solidification
Deformation
Forging
Thixoforging

20. ABSTRACT (Continue on reverse side if necessary and identify by block number)

This is the second Interim Report of a program initiated on June 24, 1976 to investigate the feasibility of producing net or near-net shape components by forging-type operations, Thixoforging, using Rheocast metals.

This report summarizes some of the findings from the first year of the program and covers the details of the investigations on high temperature alloys and results of the Thixoforging experiments in the past twelve months.

→ Over

DD FORM 1 JAN 73 1473 EDITION OF 1 NOV 65 IS OBSOLETE

UNCLASSIFIED 176 014

SECURITY CLASSIFICATION OF THIS PAGE (When Data Entered)

Block No. 20

ABSTRACT

During the past two years a number of Thixoforging systems (reheat furnaces with pentrometers and heated dies adapted to existing hydraulic presses) were designed, constructed and operated. These include: Two laboratory apparatuses with 50-ton hydraulic presses and a pilot plant size system with a 200-ton forging press.

The continuous Rheocasting apparatus was modified and located near the large press to permit direct transfer of partially solid charge material to the dies without going through a solidification and reheating cycle.

Experiments on the high temperature slurry producer showed that primary solid particle size in Rheocast cobalt-base Haynes alloy 31 and 4340 low alloy steel are of the same size as primary dendrite arm spacings in conventional specimens solidified under identical cooling rates.

A theoretical model previously developed for homogenization (solution) heat treatment of Rheocast structures was used in the heat treatment of 2024 aluminum alloy forged specimens. The specific phases in this alloy before and after homogenization heat treatment were identified using an Electron Microprobe.

An extensive theoretical and experimental program was carried out to study the effect of pressure and die coatings on the heat transfer coefficient at the die-metal (aluminum alloy) interface during the forging operation. It was found that application of 19.6×10^7Pa pressure increases the heat transfer coefficient from $\sim 3.4 \times 10^3$ $Wm^{-2}K^{-1}$ to 5.25×10^4 $Wm^{-2}K^{-1}$. The effect of different die coatings on the heat transfer coefficient were also determined.

A large number of Thixoforged parts of aluminum alloys 6061 and 2024 were produced, heat treated and their mechanical properties were determined. The disc-shaped parts, 0.12m in diameter by 0.025 to 0.04m high, produced from both Rheocast and liquid charge of 2024 aluminum alloy responded to heat treatment and possessed properties comparable to the wrought alloy. For example, tensile properties of the Thixoforged parts in the T-6 condition were $\sim$ 35Kg/mm^2 (Y.S.), 46.4Kg/mm^2 (U.T.S.) and 11.2% Elongation. These properties were slightly lower than those measured on Squeeze Cast parts made in this study. On the other hand, the fatigue properties of the Thixoforged parts were slightly superior.

FOREWORD

Technical monitor of the contract was Mr. R. Gagne.

This research was supported by the Army Materials and Mechanics Research Center, Watertown, Massachusetts, under Contract No. DAAG46-76-C-0046. Contributions from Professor M. Metzger and Dr. A. Zangvil in the analysis of second phase particles in the 2024 aluminum alloy and Dr. Y. V. Murty in the analysis of the work with cobalt-base Haynes alloy 31 are gratefully acknowledged. The 200 ton Autoforge press used in the pilot plant Thixocasting system was donated by the Doehler-Jarvis Division of NL Industries, Inc.

TABLE OF CONTENTS

		Page
	ABSTRACT	1
I	INTRODUCTION	3
II.	APPARATUS AND PROCEDURE	9
	1. Continuous Rheocasting	9
	2. Laboratory Thixoforging Apparatus	9
	3. Pilot Plant Thixoforging System	13
III.	RHEOCASTING, HEAT TREATMENT AND DEFORMATION STUDIES	15
	1. Effect of Process Variables on Rheocast Structures	15
	2. Heat Treatment Studies	19
	3. Gleeble Tests	23
IV.	DIE THERMAL BEHAVIOR	25
	1. Computer Heat Flow Calculations	26
	2. Comparison of Experiment with Theory	28
V.	STRUCTURE AND PROPERTIES OF THIXOFORGED PARTS	31
VI.	REFERENCES	35
	APPENDIX	37
	TABLE I	38
	TABLE II	39
	TABLE III	40
	FIGURES	41

ABSTRACT

This is the second Interim Report of a program initiated on June 24, 1976 to investigate the feasibility of producing net or near-net shape components by forging-type operations, Thixoforging, using Rheocast metals.

This report summarizes some of the findings from the first year of the program and covers the details of the investigations on high temperature alloys and results of the Thixoforging experiments in the past twelve months.

During the past two years a number of Thixoforging systems (reheat furnaces with penetrometers and heated dies adapted to existing hydraulic presses) were designed, constructed and operated. These include: Two laboratory apparatuses with 50-ton hydraulic presses and a pilot plant size system with a 200-ton forging press.

The continuous Rheocasting apparatus was modified and located near the large press to permit direct transfer of partially solid charge material to the dies without going through a solidification and reheating cycle.

Experiments on the high temperature slurry producer showed that primary solid particle size in Rheocast cobalt-base Haynes alloy 31 and 4340 low alloy steel are of the same size as primary dendrite arm spacings in conventional specimens solidified under identical cooling rates.

A theoretical model previously developed for homogenization (solution) heat treatment of Rheocast structures was used in the heat treatment of 2024 aluminum alloy forged specimens. The

specific phases in this alloy before and after homogenization heat treatment were identified using an Electron Microprobe.

An extensive theoretical and experimental program was carried out to study the effect of pressure and die coatings on the heat transfer coefficient at the die-metal (aluminum alloy) interface during the forging operation. It was found that application of 19.6×10^7 Pa pressure increases the heat transfer coefficient from $\sim 3.4 \times 10^3$ $Wm^{-2}K^{-1}$ to 5.25×10^4 $Wm^{-2}K^{-1}$. The effect of different die coatings on the heat transfer coefficient were also determined.

A large number of Thixoforged parts of aluminum alloys 6061 and 2024 were produced, heat treated and their mechanical properties were determined. The disc-shaped parts, 0.12m in diameter by 0.025 to 0.04m high, produced from both Rheocast and liquid charge of 2024 aluminum alloy responded to heat treatment and possessed properties comparable to the wrought alloy. For example, tensile properties of the Thixoforged parts in the T-6 condition were $\sim$ 35Kg/mm^2 (Y.S.), 46.4Kg/mm^2 (U.T.S.) and 11.2% Elongation. These properties were slightly lower than those measured on Squeeze Cast parts made in this study. On the other hand, the fatigue properties of the Thixoforged parts were slightly superior.

I. INTRODUCTION

The current emphasis on reduction of manufacturing costs by the government and industry has resulted in renewed efforts to develop new and innovative processes that would permit forming metal parts to net or near-net shapes. One such forming process, Thixoforging, has been the subject of this investigation. This program was initiated on June 24, 1976 to investigate the feasibility of producing net or near-net shape components by forging-type operations using Rheocast metals. The aim of this study was to exploit the special structure and thixotropic rheological behavior of Rheocast metals to produce porosity free, heat treatable parts, in a single forming operation, thus eliminating the substantial manufacturing costs associated with machining operations. Several areas of possible applications of such a process were envisioned. First, the deformation could be viewed as a competitive forming operation to precision casting or forging. Second, the altered metallurgical structure may permit forming of alloys that are presently only forged or only cast. Third, a most important application could be in preparation of near-net shape preforms for subsequent precision forging or machining. Finally, the process has a major advantage over processes such as die casting in that solidification of the Rheocast alloy takes place under direct applied pressures of thousands of psi (10^7 to 10^9 Pa) resulting in components free of internal porosity.

The liquid metal equivalent to Thixoforging is Squeeze Casting. This process was developed in the USSR (1,2) and has been used to produce a variety of shapes from simple gear blanks to valves with internal cored passages. Steel castings of up to 100 lbs. have been

manufactured in this way. Major advantages of this process include: production of porosity free heat treatable parts with forging properties, good surface finish, high metal utilization (absence of gates and risers), automation, etc. Some disadvantages of liquid metal Squeeze Casting include: time delay necessary for partial dendritic solidification of the liquid metal prior to pressurization (resulting in some macrosegregation), limitations in press speed due to induced turbulence in the liquid metal, difficulty in protection and transfer of high temperature liquid metals from crucible to the female die and short die life. Use of a partially solidified, Rheocast, charge material does not require further solidification in the die prior to pressurization; its high viscosity permits rapid deformation without turbulence and finally, protection and automatic transfer of a semi-solid charge is much easier than a completly liquid charge.

While it is generally recognized that pressurization during solidification enhances heat transfer across a metal-die interface, little experimental and theoretical work has been carried out to investigate this phenomenon. The heat transfer coefficient would affect die thermal behavior, hence die failure, in important ways. Therefore, a portion of this investigation dealt with the effect of applied pressure and die coatings on the heat transfer coefficient at the metal-die interface during the forging of liquid and Rheocast charge materials.

The investigation, as reported herein, can be divided into two major areas. First, the effect of process variables during slurry production, Rheocasting, on the resulting structure and the homogenization heat treatment response of ingots produced directly under

a continuous Rheocasting apparatus was studied. The aim of this work was to; (a) determine the relationship between cooling rate during slurry production and primary particle size in Rheocast specimens and compare the findings with dendrite arm spacings in conventionally cast specimens solidified under identical cooling rates, and (b) establish the necessary relationships between homogenization heat treatment times and Rheocast structures. Second, the deformation behavior of Rheocast alloys at temperatures below and above their solidus temperature was studied and Thixoforging apparatuses were developed to produce net or near-net shape components starting with a partially solid charge material. The apparatuses developed were extensively used to study the effects of process variables on heat transfer coefficients at the die-metal interface and the structure and properties of the parts produced.

The initial aim of this work was to use commercial aluminum alloys and high temperature cobalt-base and iron-base alloys for both the Rheocasting and Thixoforging experiments. However, due to the unavailability of a high power induction power supply for the reheat furnace associated with the Thixoforging apparatus, only aluminum alloys were used in forging experiments. Part of the findings from the first year of this effort were described in the first technical report (3). This report included the following:

1. Rheocast ingots of a model system Sn-15% Pb alloy and aluminum alloys 6061 and A356 were produced in a continuous slurry producer.

2. The feasibility of producing parts to net or near-net shape starting with these Rheocast ingots was demonstrated by the produc-

tion of sound flanged shaped cup parts and cylinders using a 50-ton hydraulic press equipped with controlled temperature dies.

3. Die thermal behavior was studied as a function of applied pressure by correlating experimentally measured temperatures to a computer heat flow model.

This report summarizes some of the earlier findings and covers details of the investigations on high temperature alloys and results of the Thixoforging experiments in the past twelve months of this program.

Specific areas covered include the following:

1. During the past two years a number of Thixoforging systems (reheat furnaces with penetrometers and heated dies adapted to existing hydraulic presses) were designed, constructed and operated. These include:

(a) A small laboratory Thixoforging apparatus was built which consists of: (i) a resistance furnace for reheating of Rheocast and conventionally cast charge materials, (ii) a controlled pressure penetrometer for monitoring the charge material characteristics, and (iii) a 50-ton Wabash hydraulic press which was modified to accept controlled temperature die sets for the forging experiments.

(b) The hydraulic press noted above was replaced with a more versatile electronically controlled MTS machine. This machine was modified to accept the controlled temperature die assembly.

(c) A pilot plant size (200 ton) Squeeze Casting machine, donated by the Doehler-Jarvis Division of NL Industries, was installed in our laboratories. An induction heated reheat furnace was built and equipped with a penetrometer for reheating of large (∿two lbs. or more of aluminum) charge material.

(d) The continuous Rheocasting apparatus was modified and located near the large press to permit direct transfer of partially solid charge material to the dies without going through a solidification and reheating cycle.

2. Experiments were carried out on the high temperature slurry producer to study the effect of process variables, especially cooling rate, on the structure of cobalt-base Haynes alloy 31 (alternate designation X-40) and 4340 low alloy steel.

3. Elevated temperature rapid strain rate tests, Gleeble tests, were carried out on Rheocast ingots of cobalt-base Haynes alloy 31.

4. A theoretical model previously developed for homogenization (solution) heat treatment of Rheocast structures was used in the heat treatment of 2024 aluminum alloy forged specimens. The specific phases in this alloy before and after homogenization heat treatment were identified using an Electron Microprobe.

5. An extensive theoretical and experimental program was carried out to study the effect of pressure and die coatings on the heat transfer coefficient at the die-metal interface during the forging operation. Model System Sn-15% Pb, commercial aluminum alloys 6061 and A356 were used in these experiments in both the partially solid, Rheocast and completely liquid states. Al-Si binary eutectic alloy was also used in a series of controlled experiments to better correlate the experimental conditions with the plane front solidification assumption of the computer heat flow model.

6. A large number of Thixoforged parts of aluminum alloys 6061 and 2024 were produced, heat treated and their mechanical properties were determined.

7. Rheocast ingots of cobalt base Haynes alloy 31 and 4340 low alloy steel and Thixoforged ingots of 2024 aluminum alloy were sent to AMMRC for their in-house evaluation.

II. APPARATUS AND PROCEDURE

1. Continuous Rheocasting

Partially solid, Rheocast, slurries were produced continuously in the machine shown in Figure 1. Details of this apparatus and its operating procedure have previously been reported (4). The production strategy was to melt solid metal fed continuously into the upper chamber of the machine. Simultaneously, in the lower chamber, the alloy was cooled and vigorously agitated to produce a semi-solid slurry composed of spheroidal solid particles suspended in solute enriched liquid. The slurry product exiting from the lower extremity of this machine was either cast into ingot preforms for subsequent reheating and Thixoforging operations or was collected in a heated laddle for direct transfer to the forging dies. In either operation the volume fraction of solid in the exiting slurry was controlled via direct torque measurement on the rotor and thermocouples located along the mixing chamber and at the exit port of the machine. Torque measurements were correlated to a calibrated master curve of torque versus viscosity which was predetermined on the machine using various viscosity fluids. Finally, average cooling rate during primary solidification in the lower chamber was calculated from the flow rate of the slurry and data relating volume fraction of solid to temperature in the solidification range. Volume fraction of solid in the slurry was determined by quantitative metallography of water-quenched specimens.

2. Laboratory Thixoforging Apparatuses

The two laboratory Thixoforging apparatuses used in this work are shown in Figures 2 and 3. Both systems consist of: (a) a

resistance furnace; (b) a controlled pressure penetrometer for monitoring the charge material characteristics; (c) temperature measurement and control devices; and (d) a hydraulic press containing a controlled temperature die set. The hydraulic unit in the apparatus shown in Figure 2 is a 50 ton Wabash press, while the one in Figure 3(a) is an MTS machine with its associated controls which was modified to accept the die assemblies used in the forging experiments.

The resistance furnace for reheating, partial or complete melting, of the charge material is shown on the left side of Figure 2(a) and consists of a vertical cylindrical chamber, 0.06m in diameter and 0.12 m long. Its temperature is controlled to ± 1K. The charge material contained in an alumina crucible can be moved out of the furnace by a hydraulic jack located below it. This furnace with the penetrometer mounted above it was used with both presses shown in Figures 2(a) and 3(a).

The penetrometer consists of a 3.2×10^{-3}m diameter alumina rod attached at one end to a small air cylinder. The lower end of the penetrometer rests on top of a slug of the charge material and exerts a controlled amount of pressure on the slug. It is calibrated to penetrate slugs of partially solid materials at a given velocity when the slugs reach a desired volume fraction solid during the heating cycle. Calibration, pressure setting, was done by locating two thermocouples in the slug, one near the center and one close to the edge. During reheating cycle of the various partially solid charge materials, the penetrometer was the primary control for determining when the charge was ready for the forging operation. The temperature in superheated liquid charge materials

was monitored by a thermocouple located in the alloy. Once a charge material was deemed ready for the forging operation, it was manually transferred to the lower cavity of the die in one of the hydraulic presses.

H-19 and H-13 steel dies were used to produce a flanged shaped cup part, Figures 2(b), 3(b) and 4(b), and unidirectionally solidified cylinders, Figures 4(c), 4(d) and 5. The dies were preheated to the desired temperature via six or more 1000 Watt cartridge and cylindrical resistance heaters. Die temperatures were closely monitored via a control device coupled to the heaters. In the first year of the program the cylindrical die assembly shown in Figures 4(c) and 4(d) was used which contained an H-13 steel ejector cylinder located at the bottom of the lower die. Thermocouples were press fitted in this piece at various distances from the die-metal interface. Essentially, unidirectional solidification was achieved by insulating the sides of the lower die and the bottom of the top die. Once a charge material, liquid or partially solid was placed in the lower die, the ejector cylinder containing the thermocouples began heating and the effect of pressure was only recorded after the two die halves were closed. Thus, thermal profiles obtained were in two distinct regimes, one before and one after pressurization. This necessitated the use of two different heat transfer coefficients in the computer heat flow model to simulate heat flow in each regime. In order to alliviate this problem, the alternate cylindrical die design shown in Figure 5 was used in the second year of the program. In this design the thermocouples are located in the cold top die half and die thermal behavior is recorded simultaneously with pressurization. Therefore, a single heat transfer coefficient is used

in the computer heat flow model for a given set of experimental variables (pressure and die coating).

In experiments designed to determine the heat transfer coefficients at the die-metal interface, the lower die was heated to ∿700K while the upper die was kept at room temperature. The lower die surface was insulated with a layer of fiberfrax and a mixture of clay and high temperature cement. The bottom surface of the upper die was polished with a 600 grit paper and treated by one of the following methods prior to the forging operation:

(a) No coating was applied.

(b) The surface was coated by acetylene soot to a thickness of about 0.05mm.

(c) A mixture of graphite powder and isopropyl alcohol (prepared from dilution of "Dag 154"* with the alcohol 1:20) was sprayed on the surface for a period of about 3 seconds. The thickness of the coating was approximately 0.05mm.

(d) The same mixture as in (c) above was sprayed for 10 seconds, building up a coating of about 0.2mm on the surface.

(e) A mixture of die release agent and water (prepared by diluting a release agent 1163* with water 1:40) was sprayed on the surface for 3 seconds.

Thixoforged flanged shaped cup parts and unidirectionally solidified cylinders were produced in both apparatuses with model system Sn-15% Pb alloy, commercial aluminum alloys 2024, A356 and 6061. Die thermal behavior was studied with Sn-15% Pb alloy, commercial aluminum alloys A356 and 6061 and Al-Si binary eutectic alloy.

---

*Supplied by Acheson Company, Port Huron, Michigan 48060

3. Pilot Plant Thixoforging System

This system consists of; (a) an induction powered (∿4KW) reheat furnace; (b) a controlled pressure penetrometer; (c) temperature measurement and control devices; and (d) a fully automated 200 ton AutoForge specially modified for use in Squeeze Casting and Thixoforging. Photographs of this system are shown in Figure 6. Figure 6(a) shows an overall view of the apparatus which includes the reheat furnace and its associated power supply. A photograph of the reheat furnace with the controlled pressure penetrometer located on top of it is shown in Figure 6(b). Rheocast ingots are placed in an alumina crucible, 0.1m in diameter and 0.17m tall. This crucible rests on a table which is counter weighed and moves up and down vertically on two bearings riding on vertical rods. The motion of the table is electronically coupled to the penetrometer.

The charge is again manually transferred from the reheat furnace to the dies. The temperature of each Rheocast ingot was initially monitored with two thermocouples located at the center and one extremity of the ingot. The power input to the induction coil was altered during a reheating cycle such that no more than a 1 to 2K temperature differential was noted between the two thermocouples. The penetrometer was again calibrated to penetrate the Rheocast ingots at a given velocity when the slugs reached a given volume fraction of solid. Temperature for the superheated liquid charge material was monitored by a single thermocouple located in the alloy.

A large number of experiments were carried out with this apparatus using Rheocast ingots of 2024 aluminum alloy weighing approximately one killogram. Metallographic examination of the disc

shaped parts (∿0.12m in diameter by 0.025 to 0.04m tall) revealed that some of the surface oxides on the Rheocast ingots were entrapped within the parts. This was deemed undesirable and an alternate Thixoforging approach was developed for the production of high quality, heat treatable parts with little or no entrapped oxides. In this approach the continuous Rheocasting machine was redesigned with a larger lower mixing chamber and was relocated near the forging press as shown in Figure 7(a). Partially solid charge material was intermittently collected in the coated stainless steel ladles shown in Figure 7(b) and directly transferred to the lower die shown in Figure 7(c). The ladles were initially preheated to a temperature of ∿ 500K to avoid further solidification during charge collection and transfer. Rheocast Charge collection and transfer was synchronized with the operation of the forging press to permit Thixoforging of aluminum alloy parts every few minutes. The dies were coated after each forging operation with a mixture of graphite powder and isopropyl alcohol (coating (c) described in the previous section). Thixoforged discs of 2024 aluminum alloy produced are shown in Figures 7(b) and 7(c). Finally, part thickness was varied by changing the ladle height as shown in Figure 7(b).

III. RHEOCASTING, HEAT TREATMENT AND DEFORMATION STUDIES

The general aim of this portion of the investigation was to; (1) determine the relationship between cooling rate during slurry production and primary particle size in Rheocast specimens and compare the findings with dendrite arm spacing in conventionally cast specimens solidified under identical cooling rates; (2) establish the necessary relationships between homogenization heat treatment times and Rheocast structures; and (3) study the deformation behavior of Rheocast alloys below their solidus temperatures.

1. Effect of Process Variables on Rheocast Structures

The two alloys used in this study were cobalt-base Haynes alloy 31 (alternate designation X-40) and AISI 4340 low alloy steel*. The former alloy was used in concurrent studies in this program and another program sponsored by the Department of Defense which was reported separately (4,5). The 4340 low alloy steel was only investigated in this program.

Previous fundamental (6) and applied (4,5,7) studies on the effect of process variables during Rheocasting on the structure and the rheological behavior of partially solid slurries has shown that:

(a) The structure of a partially solidified, vigorously agitated metal slurry is a function of the process variables (cooling rate, shear rate and volume fraction solid). That is, the size, distribution of size, shape of the primary solid particles and the volume fraction of entrapped liquid in these particles can be significantly altered by varying the processing conditions. For example,

---

* The nominal compositions of these two alloys are: cobalt-base Haynes alloy 31 (Co-26.5% Cr - 10.5% Ni - 7% W- 0.5%C), AISI 4340 low alloy steel (Fe 0 0.7% Mn - 0.25% Mo - 0.8% Cr - 1.85% Ni - 0.3% Si - 0.4% C - .035% max. p - 0.04% max.S).

increasing the average cooling rate makes the primary solid particles more uniform and smaller in size, but increases the amount of entrapped liquid in each particle - increases the effective volume fraction of solid in the slurry, hence increases its viscosity (4-7).

(b) The thixotropic behavior of a metal slurry as quantitized by a measure of the hysteresis loop, determined on a high temperature viscometer, is a function of the structure as well as the conditions under which the loop is generated (6).

(c) The rheological properties of a metal slurry are similar to those of many well known non-metallic suspensions (6).

One important finding from the previous studies (4,5) on a low temperature Sn-15% Pb alloy was that primary dendrite arm spacings in conventional castings and primary particle size is continuously produced slurries are of the same order of magnitude if the average cooling rates during solidification are identical, Figure 8.

This observation was confirmed in the high temperature alloys used in the present investigation. The results obtained for the cobalt-base alloy and the low alloy steel are shown in Figures 9 and 10, respectively.

The relationships between primary and secondary dendrite arm spacings and average cooling rate in these high temperature alloys were determined from directionally solidified ∿0.13m tall ingots in which six or more thermocouples were located at different distances from the bottom chill. The measured dendrite arm spacings close to the thermocouple locations were then correlated to the average cooling rates recorded during solidification. As anticipated, measured dendrite arm spacings were inversely proportional to average cooling

rate to an exponent. For each alloy the relationship is given by:

$$d = b(\varepsilon_{Avg})^{-n} \qquad (1)$$

where d is primary or secondary dendrite arm spacing in microns, b and the exponent n are constants (different constants for primary and secondary dendrite arm spacings), and ε_{Avg} is the average cooling rate during solidification.

The constants in equation (1) for the two alloys were calculated from Figures 9 and 10. The equations for the cobalt-base Haynes alloy 31 are:

$$\begin{aligned} d &= 90\ \varepsilon_{Avg}^{-0.32} \quad \text{Primary} \\ d &= 40.4\ \varepsilon_{Avg}^{-0.27} \quad \text{Secondary} \end{aligned} \qquad (2)$$

The equations for the 4340 low alloy steel are:

$$\begin{aligned} d &= 245\ \varepsilon_{Avg}^{-0.3} \quad \text{Primary} \\ d &= 116\ \varepsilon_{Avg}^{-0.29} \quad \text{Secondary} \end{aligned} \qquad (3)$$

The effective average primary particle size, p.p.s., in the slurries were determined from specimens water quenched directly under the continuous slurry producer. Figures 11(a) and 12 show the Rheocast and water-quenched structures of the cobalt-base Haynes alloy 31 and the 4340 low alloy steel, respectively. Note the difference between the structures in Figures 11(a) and 11(b). The former was water-quenced as it exited from the slurry producer while the latter was cast in an ingot mold. The rapid solidification experienced by the remaining solute enriched liquid during the water

quench resulted in the fine dendritic structures which delineate the primary solid particles.

The average cooling rate during primary solidification in the lower mixing chamber of the slurry producer was calculated from the following equation:

$$\varepsilon_{Avg} = \Delta T_s(g_s)/t_r(g_s) \qquad (4)$$

where g_s is the volume fraction of the primary solid particles in the slurry determined by metallography, $\Delta T(g_s)$ is the difference between the liquidus temperature and the temperature of the exiting slurry determined by locating a thermocouple in the direct path of the exiting slurry, and $t_r(g_s)$ is the average residence time of the alloy in the mixing chamber determined from the volume of the mixing chamber and the measured average flow rate of the slurry.

Note that the data in Figures 9 and 10 are for effective volume fraction solid, g_s, in the slurry in the range of 0.45 to 0.6 and average shear rate during slurry production of $\sim$600 sec^{-1}. The plots in Figure 10 also include data from Bye (7) who has carried out an extensive study of the rheological behavior of 4340 low alloy steel confirming earlier findings of Joly and Mehrabian (6).

Finally, it should be noted that the primary particle size in Rheocast slurries is also a function of shear rate and volume fraction of solid. It decreases with increasing shear rate at low cooling rates and increases with increasing volume fraction of solid in the slurry (5,6,7).

2. Heat Treatment Studies

The effect of cast (Rheocast) structures on microsegregation and heat treatment response of the two high temperature alloys and commercial 2024 aluminum alloy were studied. A portion of this work has overlapped with a previous program sponsored by the Department of Defense (4,5). As example, the theoretical model for solution heat treatment of Rheocast structures previously reported (5) was developed for both investigations. However, work in this area, especially identification of insoluble second phases, was continued in the present program and will be reported in detail herein. On the other hand, only a summary of the earlier findings will be given where appropriate.

In general, electron probe microanalysis of water quench Rheocast slurries show a relatively flat composition profile of alloying elements in the primary solid particles with abrupt changes in their boundaries. For example, note the concentration profiles of chromium, nickel and tungsten versus position in the primary solid particle of cobalt-base Haynes alloy 31 shown in Figure 13. This segregation profile differs from conventional dendritic microsegregation where a minimum or maximum concentration is usually observed at the center of dendrite arms. During high temperature heat treatment significant solute redistribution and second phase dissolution was expected and observed. Some of the primary carbide phase in the interparticle boundaries dissolved and reprecipitated as $M_{23}C_6$ type carbides during very slow cooling from the heat treatment temperature. Increased carbide dissolution, diffusion of solute elements into the primary solid particles, carbide reprecipitation and coarsening were noted with increasing heat treatment times. Microhardness

measurements carried out across the primary solid particles of the as-Rheocast and heat treated specimens shown in Figure 14 confirmed these observations.

Similar trends were noted in the 4340 low alloy steel specimens. Chromium, manganese and nickel showed some positive segregations in the interparticle spaces which were significantly reduced after homogenization heat treatment.

Analytical and computer models were developed for solutionizing of Rheocast and conventional cast (dendritic) alloys. The details of this model have been reported (5). As in the case of dendritically solidified structures, the critical dimensionless parameter for dissolution of non-equilibrium second phase particles and solute redistribution is $[D_s t/\ell^2]$. Where D_s is the diffusion coefficient of solute atoms at the heat treatment temperature, t is the time of heat treatment, and ℓ is a characteristic distance over which microsegregation manifests itself. In dendritic solidification ℓ is one-half the dendrite arm spacings while in Rheocast structures it denotes the radius of the primary solid particles.

Experiments were carried out on commercial 2024 aluminum alloy to verify the prediction of the model. Figure 15 shows the experimental measured variation in the volume fraction of interdendritic phase as a function of solutionizing time at 788K for the Rheocast and the conventional cast commercial 2024 aluminum alloy. Although the curves for each processing mode exhibits similar characteristics, the initial volume fraction for the Rheocast alloy is only 0.062 whereas the initial volume fraction for the dendritic material is 0.075. After 50 hours, however, both materials retain approximately 0.014 volume fraction of interdendritic or inter-particle phases.

Since little change is detected between the amount of interdendritic and inter-particle phases after heat treatment for 10 to 50 hours, one can conclude that 0.014 is the equilibrium fraction at the heat treatment temperature of 788K.

Figure 16 shows the results of the diffusion simulation for the solidification and solutionization of Rheocast commercial 2024 aluminum alloy. The general shape of both the numerical simulation and the analytical curves is similar; however, the analytical curve predicts that at any dimensionless time more dissolution will occur than is predicted by the numerical technique. Of the two curves the numerical simulation technique agrees most closely with the experimental points, particularly at short times.

One important implication of the findings from this work was that for a given value of dimensionless time, $D_s t/r_o^2$, the spherical Rheocast structure solutionizes faster than the plate-like dendritic structure (5). The increase in dissolution rate of Rheocast structures is due to the spherical geometry which provides a larger surface area of the second phase/primary solid interface per unit volume than that for any other simple geometrical shape.

Due to the high solutionization temperature, 788K, used in the earlier concurrent investigations some incipient melting of the interdendritic eutectic phase was noted in the commerical 2024 aluminum alloy. Furthermore, only preliminary studies were carried out to identify the soluble and insoluble second phases. These investigations were continued in the present program to better identify the composition of the second phases, especially the iron-rich phases, prior to and after solutionization at a lower temperature of 778K.

A JEOL Type 50A Electron Microprobe was used. The data from the microprobe was corrected for absorption coefficient, atomic number and fluorescence via a computer program especially designed for this purpose.

In the as-Rheocast condition the following second phases were identified: $CuAl_2$, $CuMgAl_2$, α(Al-Fe-Mn-Si) which contains some Cu and (Cu-Fe-Mn)Al_6. The composition of the second phases were quantitatively and qualitatively established using the electron microprobe and the associated elemental x-ray maps, respectively. Figure 17 shows Secondary Electron Images of the eutectic in the as-Rheocast structure. The SEI's of the ternary eutectic α + $CuAl_2$ + $CuMgAl_2$ and the binary eutectic α + $CuAl_2$ are shown in Figures 17(a) and 17(b), respectively. In addition to the microprobe data a differential etching technique was used to identify the $CuMgAl_2$ phase in the ternary eutectic. The etchant was a 10% H_3PO_4 water solution which darkened the $CuMgAl_2$ phase without affecting the $CuAl_2$.

Figure 18 shows a Secondary Electron Image and the associated X-ray elemental maps of the α[Al-Fe-Mn-Si] phase. The average composition of this phase from electron microprobe analysis was ∿74 at %Al - 8.5 at %Fe - 2.5 at %Cu - 7.5 at %Mn - 7.5 at %Si. Figure 19 shows a Secondary Electron Image and the associated x-ray elemental maps of a (Cu-Fe-Mn)Al_6 type particle. The elemental x-ray maps in Figure 19(c) and (d) show high concentrations of Fe and Mn in the particles, while the Cu map shows higher concentrations of copper in the eutectic phase. The average compostion of the α(Fe-Cu-Mn)Al_6 from microprobe analysis was ∿84 at %Al - 2.5 at %Cu - 7 at %Fe - 6.5 at %Mn.

During short solutionizing heat treatment (∿½ hour) at 778K.

significant dissolution of the $CuMgAl_2$ phase was noted leaving behind nearly pure α + $CuAl_2$ eutectic. Most of the $CuAl_2$ second phase particles disappeared as solutionizing time was increased to 50 hours. Dissolution of $CuMgAl_2$ and $CuAl_2$ during solution heat treatment accounts for most of the measured drop in the overall volume fraction of the second phases in Figures 15 and 16. The α(Al-Fe-Mn-Si) phase which contains some Cu did not dissolve during solutionization. However, the (Cu-Fe-Mn)Al_6 type phase could not be detected in the structure after a heat treatment of $\sim$10 hrs. at 778K. A new iron-rich phase, possibly Cu_2FeAl_7, was observed in the 10 hr. solutionized specimens.

It is postulated that this new phase is due to modification of the existing (Cu-Fe-Mn)Al_6 phase during the homogenization heat treatment. These latter observations are in contrast to those reported in our earlier investigations (5).

Identical phases to the above were also noted in the conventional dendritic as-cast and homogenized specimens of the commercial 2024 aluminum alloy.

3. Gleeble Tests

Elevated temperature rapid strain rate tensile tests, Gleeble tests, are generally used to determine the hot working characteristics (ductility and strength) of alloys. Rheocast ingots of the cobalt-base Haynes alloy 31 were sectioned longitudinally and machined into Gleeble test specimens 6.35×10^{-2}m (1/4") in diameter by 8.89×10^{-2}m (3 1/2") long. These were tested at Cabot Corporation in Kokomo, Indiana. The specimens were heated to the test temperature at a rate of 222K/sec. Specimen temperature was monitored by a thermocouple spot welded to its surface. Crosshead speed of 2.54×10^{-2} m/sec were used. The ultimate load, apparent

yield load, and reductions in area were measured. The data obtained is shown in Figures 20 and 21, Data available on dendritically solidified specimens from the literature (8) is also shown on these plots. The hot ductility of the air melted Rheocast ingots were consistently lower than that reported in the literature for investment cast or electroslag remelted ingots (8,9) while the yield strengths were slightly lower. Metallographic examination of the Rheocast specimens showed that the failures originated from distributed porosity in the Rheocast ingots. This was expected since the ingots were produced from a 0.5 volume fraction solid slurry without application of pressure in a relatively cold mold.

Table I shows compiled data of tensile and stress rupture properties of cobalt-base Haynes 31 alloy from previous investigations (5,10). These data show that internal porosity in as-Rheocast ingots and thin foil die castings affects ductility and stress-rupture properties adversely. Data in Table I also show that hot isostatic pressing of Rheocast ingots and Thixocast airfoils closes the internal porosity - improves stress-rupture life significantly. As noted in a subsequent section of this report, Thixoforging combines the net shape forming of a casting process with the high pressure (porosity free) forming of a forging process.

IV. DIE THERMAL BEHAVIOR

The theoretical and experimental investigation of die thermal behavior during forging of liquid and partially solid aluminum alloys previously initiated (3) was continued and expanded to include the effects of applied pressure and die coatings on the heat transfer coefficient at the metal-die interface. Both the die geometry and the aluminum alloy used were altered in this work to get closer agreement between the assumptions of the computer model and the experiments.

Figures 22 and 23 show the recorded die temperatures during forging of superheated liquid and partially solid commercial 6061 and A356 aluminum alloy charge materials, respectively (3). The applied pressure was $\sim 9.1 \times 10^7$ Pa. The data in these Figures show an abrupt jump in recorded die temperatures due to pressurization - the vertical arrows indicate time of pressurization. The data in Figures 22 and 23 also show that there was 10 to 50K difference between the highest die temperatures recorded when the charge was partially solid and completely liquid. This temperature difference can be attributed to the difference in the initial charge temperature rather than any significant difference between the heat transfer coefficients at the die-metal interface. This fact is deduced from the heat transfer coefficients listed in Figures 24 and 25 for the completely liquid and partially solid charge materials, respectively, of the commercial A356 aluminum alloy.

A one-dimensional computer heat flow program was developed to simulate the heat flow in the unidirectionally solidified cylindrical part and the steel dies. From the correlation of computer prediction and measured temperatures, it was found that the heat transfer

coefficient increases by one order of magnitude or more upon application of 9.1×10^7 Pa pressure. Heat transfer coefficients before and after pressurization were 3.4×10^3 and 3.4×10^4, respectively, for a liquid and 8.4×10^2 and 3.1×10^4 $w \cdot m^{-2} \cdot k^{-1}$, respectively, for a partially solid A356 aluminum alloy (3).

In the second year of this program the alternate cylindrical die design shown in Figure 5 was used. In this design the thermocouples are located in the cold top die half and the die thermal behavior is recorded simultaneously with pressurization. Therefore, a single value of heat transfer coefficient is used to correlate the computer heat flow model with the experimental findings. Since no significant difference in die thermal behavior was noted between the partially solid and liquid charge materials, Al-Si alloy of eutectic composition was used in this work to better simulate the discrete liquid-solid interface position assumed in the computer heat flow model. Finally, the computer heat flow model was slightly modified to account for the altered die geometry employed in this study.

1. Computer Heat Flow Calculations

Heat transfer coefficients were calculated by matching computer simulated and experimental die thermal response curves. The details of the computer heat flow model were previously reported (3,11). Hence, only a brief description of the model and the changes made will be given here.

The mathematical problem is presented by the one-dimensional thermal diffusion equation:

$$\frac{k}{\rho} \frac{\partial^2 T}{\partial x^2} = \frac{\partial H}{\partial t} \qquad (5)$$

where H, T, t, ρ and k represent the enthalpy, temperature, time, density and thermal conductivity, respectively. The boundary and initial conditions employed are:

$$
\begin{aligned}
&1) \quad x = L_C;\ \frac{\partial T}{\partial x} = 0 \\
&2) \quad x = 0;\ \frac{\dot{Q}}{A} = h\Delta T_s \\
&3) \quad t = 0,\ 0 < x < L_C;\ T = T_0 \\
&4) \quad t = 0,\ -L_D < x < 0;\ T = T_D
\end{aligned}
\qquad (6)
$$

where T_D and T_0 are the initial die and metal temperatures, respectively, ΔT_s is the temperature difference at the metal-die interface. The ratio $\dot{Q}/A$ represents the rate of heat flow through a perpendicular surface of unit area. L_D and L_C are the die thickness and forging thickness, respectively.

The thermal diffusion equation, expression (5), was solved using a forward difference technique with the boundary conditions (6) also reduced to the finite difference form.

The construction of the solution to the problem involved the incorporation of the following assumptions:

1) Pressurization commences instantaneously after a fixed time following lower die filling.
2) The upper die with the thermocouples is initially at a uniform temperature and undergoes no phase transformation on heating.
3) The heat transfer coefficient remains constant during pressurization.
4) The physical properties of the liquid metal are independent of temperature.

5) From the physical geometry and location of the die assembly and thermocouples any other heat flux could be incorporated by a heat input proportional to the difference in temperature of that location and the ambient.

The simulated version of the response curve was constructed after monitoring temperatures at fixed nodal points corresponding physically to thermocouple locations in the casting and the die. Thirteen nodal points along the length of the die and eleven nodal points along the vertical axis of the casting were used. The thermophysical properties of the materials used are given in the Appendix. Finally, a CYBER 175 computer was used and calculated temperatures were documented every 0.2 seconds.

2. Comparison of Experiment With Theory

A number of unidirectional heat flow experiments were carried out to determine the effect of pressure and die coatings on the heat transfer coefficient, h, at the metal-die interface. The applied pressure was varied from $\sim 10^7$ pa to $\sim 20 \times 10^7$ Pa. Five different die coatings were used as described in a previous section. In order to obtain agreement between computer predictions and the experimentally determined temperature profiles, several computer simulations were carried out using different values of h for each experiment.

Representative plots of the experimentally recorded temperatures at different locations from the metal-die interface at a high applied pressure of 19.7×10^7 Pa is shown in Figure 26. Figure 27 shows the results from a computer simulation and experimentally determined die temperatures. The applied pressure in this experiment was 13.1×10^7 Pa and the die was coated with a 0.05mm thick mixture of graphite powder and isopropyl alcohol. In general, the agreement between

the thermal response of the thermocouples at 1mm and that of the computer was excellent. However, it was found that heat input from the lower die half after pressurization affected the thermal response of the other thermocouples located at 4 and 10mm from the metal-die interface. Therefore, a heat input consistent with assumption (5) of the computer heat flow model was introduced to obtain the close match between the measured and simulated temperature profiles shown in Figure 27. The assumed side heat transfer coefficient for this case was 1.87×10^4 $Wm^{-2}K^{-1}$. This value is reasonable because a thin layer of liquid metal was consistently pushed into the gap between the sides of the two die halves.

Data similar to those in Figure 27 were generated for all of the heat transfer coefficients reported below.

(a) Effect of Applied Pressure

The effect of applied pressure on the thermocouple located at 1mm from the metal-die interface is shown in Figure 28. As expected, increasing the applied pressure resulted in a corresponding increase in the recorded die temperatures. A plateau followed by a second temperature rise was noted for the lower applied pressures. This observation may be associated with the formation and subsequent collapse of a gap at the metal-die interface at the initial stages of solidification. However, no definite explanation of this phenomena can be offered at this time.

Figure 29 shows the effect of applied pressure on the heat transfer coefficients at the metal-die interface. Data from the first year of this investigation on commercial A356 aluminum alloy are included in this Figure. In general, the data show that heat transfer coefficient for a given die coating increases with increasing

applied pressure. The highest heat transfer coefficient, h = 5.25 x 10^4 Wm^{-2} K^{-1}, was obtained for an applied pressure of 19.7 x 10^7 Pa. Finally, there is a general trend in these curves indicating a diminishing effect of pressure on the heat transfer coefficient with increasing pressures.

(b) Effect of Die Coatings

The effects of various die coatings on the die temperature and the heat transfer coefficient at the metal-die interface are shown in Figures 29 and 30. As anticipated, the highest die temperatures recorded were for the case of no die coating, curve (a) in Figures 29 and 30. Acetylene sooth, curves (b), produced the second lowest resistance to heat flow at the interface, while increasing the thickness of the graphite powder-isopropyl alcohol mixture from 0.05mm to 0.2mm resulted in a corresponding increase in the resistance to heat flow - note the decrease in the heat transfer coefficients from curves (c) to (d) in Figures 29 and 30.

Finally, the values of heat transfer coefficients determined in this study appear to be in reasonable agreement with those reported in a study by Y. Nishida et al (15). They reported values of 0.42 x 10^4 and 4.2 x 10^4 for applied pressures of 0.5 x 10^6Pa and 6.5 x 10^7Pa, respectively, during Squeeze Casting of pure aluminum.

V. STRUCTURE AND PROPERTIES OF THIXOFORGED PARTS

The two laboratory Thixoforging apparatuses, Figures 2 and 3, and the pilot plant size Thixoforging system, Figures 6 and 7, were used to produce a large number of flanged cup, cylindrical and disc shaped parts. The commercial alloys used were 2024, A356 and 6061 aluminum alloys. The alloys were used both when the charge was completely liquid, Squeeze Casting, and partially solid, Thixoforging. The parts were examined metallographically for soundess and microstructural characterization. Tensile properties were determined on both the Squeeze Cast and Thixoforged parts. Some of the data generated in the first year of this effort was previously reported (3) and will be only summarized herein. All the experiments on the pilot plant system, which permits applications of pressures as high as 2.1×10^8Pa on a 0.12m diameter disc shaped component, were carried out in the second year of this investigation.

The microstructures of flanged cups produced in the laboratory apparatuses from partially solid and superheated liquid 6061 aluminum alloy charge materials are shown in Figure 31. Figure 31(a) shows the characteristic structure of a Thixoforged material. Each grain resulted from coarsening of a primary solid particle in the initial slurry. The dendritic structure of Figure 31(b) is that expected from conventional solidification of a completely liquid charge. The microstructures of unidirectionally solidified cylinders of commercial A356 aluminum alloy produced from a partially solid and a completely liquid charge material are shown in Figure 32.

Similar unidirectional castings to that shown in Figure 32(b) were produced using commercial 2024 aluminum alloy with and without applied pressure. These experiments were done to ascertain whether

the increased heat transfer coefficient at the metal-die interface could induce a corresponding refinement of the microstructure near the interface. Measured primary dendrite arm spacings at 2mm and 8mm from the metal-die interface were 28μm and 40μm, respectively, when no pressure was applied during solidification. Application of 8.8×10^7 Pa pressure resulted in a significant refinement of the microstructure. The measured primary dendrite arm spacings for the same two locations were 13μm and 20.5μm, respectively.

Flanged cup parts of commercial 6061 aluminum alloy made in the laboratory apparatus from both liquid and partially solid material were sectioned, heat treated and tested for tensile properties. Average tensile data from several specimens are listed in Table II. These data show that porosity closure during Thixoforging of previously Rheocast ingots improves the ductility of the alloy. However, as previously noted, some of the oxide from the ingot surface was entrapped in the forgings reducing the overall measured ductility - compare percent elongation in the Thixoforged parts with that reported for the wrought alloy in Table II. On the other hand, measured strengths of both the Thixoforged and the Squeeze Cast specimens exceed the reported values for the wrought alloy heat treated to a T-6 condition.

Most of the experiments in the pilot plant system were done with commercial 2024 aluminum alloy. Initially, all the partially solid charge material was Rheocast into 0.075m diameter ingots, reheated and Thixoforged in the apparatus shown in Figure 6. However, metallographic examination of the parts produced revealed that some of the surface oxides on the Rheocast ingots were again entrapped within the forged components. As previously noted, all subsequent specimens were produced using the apparatus and charge transfer mechanism

shown in Figures 7(a) and 7(b). A typical microstructure of the Rheocast and water quenched alloy is shown in Figure 33. The volume fraction of solid in this material was $\sim$ 0.55. Thixoforged discs were produced by direct transfer of this type of charge material to the lower die of the forging press. A typical Thixoforged commercial 2024 aluminum alloy disc and its associated microstructure prior to heat treatment are shown in Figures 7(b), 7(c) and 34. No porosity or significant oxide entrapment was noted in these two parts. Similar disc-shaped parts were also produced from an initially superheated liquid charge material. Typical microstructures of both Squeeze Cast and Thixoforged parts are shown in Figure 35. The structures are almost identical except the primary solid particles, better delineated in Figure 33, are still discernable in the microstructures of Figure 35(a) and 35(b).

Both the tensile and fatigue properties of the Thixoforged and Squeeze Cast parts were determined after heat treatment. All the specimens were first solutionized for twenty-four hours at 768K. The tensile specimens were subsequently aged to a T-6 condition while fatigue tests were carried out on the as-solutionized specimens, T-4 condition. Table III lists the tensile properties of both Thixoforged and Squeeze Cast parts. While the average tensile properties of Thixoforgings are slightly lower both sets of properties are comparable to the properties reported for wrought commercial 2024 aluminum base alloy (12).

The fatigue life tests on the Thixoforged and Squeeze Cast commercial 2024 aluminum alloy parts were conducted on a MTS Series 300 four-column Load Frame at room temperature. The unnotched specimens underwent stress (load) controlled compression - tension

cycles with a zero mean and a constant frequency of 300 cpm. The tests were conducted under different stress levels in the range of $\sim$ 10 to 25 Kg/mm^2. Under each stress level, the number of cycles that the specimen withstood before fracture was recorded, and the test was repeated three times at the same stress level before a reliable average fatigue life was obtained. Two types of specimens, Figure 36(a) and 36(b) were used in these tests. Both specimens are cylindrical in shape and are threaded at both ends. The one shown in Figure 36(a) has a uniform test section. The other one with a continuous radius between ends, shown in Figure 36(b), was used to avoid plastic buckling at high stress levels. Finally, the surface of each specimen was polished down with a 600 grit SiC paper prior to testing.

The fatigue test results are plotted in Figure 37. The Thixoforgings consistently showed slightly higher resistance to fatigue failure compared to the Squeeze Cast parts.

VI. REFERENCES

1. V. M. Plyatskii, Extrusion Casting, Primary Sources, New York, N.Y., 1965.

2. A. I. Batyshev, E. M. Bazilevskii, Yu. A. Evstratov, V. K. Zabaluev, F. A. Martynov and Yu. S. Pugin, "Casting Copper Alloys with Solidification Under Piston Pressure," Russian Castings Production, pp. 220-223, June, 1972.

3. R. Mehrabian, S. D. E. Ramati, G. J. Abbaschian and D. G. Backman, "Structure and Deformation Characteristics of Rheocast Metals," Annual Report, December 1977, Contract No. DAAG46-76-C-0046, AMMRC CTR-77-30, 24 June 1976 to 23 June 1977, prepared for Army Materials and Mechanics Research Center, Watertown, Mass.

4. R. Mehrabian, D. G. Backman, Y. V. Murty, G. J. Abbaschian, S. D. E. Ramati, S. Hong and R. J. Lauf, "Machine Casting of Ferrous Alloys," Semi-annual Technical Report, ARPA Contract No. DAAG46-76-C-0023, 1 April 1976 to September 30 1976, prepared for Army Materials and Mechanics Research Center, Watertown, Mass.

5. R. Mehrabian, D. G. Backman, G. J. Abbaschian, C. Y. Chen, S. Hong, S. D. E. Ramati and Y. V. Murty, "Machine Casting of Ferrous Alloys," Final Report, ARPA Contract No. DAAG46-76-C-0023, AMMRC CTR-78-23, 1 October 1975 to 31 December 1977, prepared for Army Materials and Mechanics Research Center, Watertown, Mass.

6. P. A. Joly and R. Mehrabian, J. of Materials Science, Vol. 11, 1976, p. 1393.

7. R. L. Bye, Jr., "Rheocating in Low Alloy Steel," M. S. Thesis, Department of Materials Science and Engineering, Massachusetts Institute of Technology, February, 1978.

8. COBALT, No. 50, March 1971, pp. 20-25.

9. "Gleeble hot ductility of Haynes Alloy No. 31", Cabot Corporation, Kokomo, Ind.

10. L. F. Schulmeister, et al., Proceedings of AMMRC Workshop on Rheocasting, February, 1977.

11. D. G. Backman, R. Mehrabian and M. C. Flemings, Met. Trans. B., Vol. 8B, 1977, p. 471.

12. ALUMINUM, Vol. I, American Society for Metals, Metals Park, Ohio.

REFERENCES cont'd

13. Handbook of Binary Metallic Systems, Structures and Properties, Editorial Board of Institute of Metallurgy of Academy of Science of the U.S.S.R. Chief Editor, N. V. Ageev, Moscow, 1959. Translated from Russian by Israel Program for Scientific Translations, Jerusalem, 1966.

14. S. C. Schaefer, Thermodynamics of Al-Si System, Rep. Invest No. 7895, U. S. Department of Interior, Bureau of Mines, Washington, D.C., p. 15.

15. Y. Nishida and H. Matsubara, Br. Foundry Man., Nov., 1976, 69 (11), pp. 274-278.

APPENDIX

Thermophysical Properties used in Computer Simulations. From References (12-14)

Density — The values of density for the H-13 and the aluminum alloy are 7800 and 2660 Kg/m^3, respectively.

Thermal Conductivity

Steel = 33.5 W/m K

Al-Si Eutectic = 162 W/m K

Enthalpy — The variation in Enthalpy in J/Kg with temperature for the steel die and the aluminum was represented by:

$$\text{Steel: } \Delta H = 684.6T - 2.13 \times 10^5 \quad (T > 304K)$$

$$\text{Al-Si Eutectic: } \Delta H = 739.6T + 0.226T^2 - 2.41 \times 10^5 \quad (298K < T < 850\ K)$$

$$H = 947.1T - 2 \times 10^5 \quad (T > 850\ K)$$

TABLE I

(a) Properties of Cobalt Base Haynes Alloy 31 Ingots (From Reference 5)

Property	As-Rheocast	Investment Cast	Design Minimum
0.2% Tensile Yield Strength (Kg/mm^2)	54.2	53.5	35.2
Ultimate Tensile Strength (Kg/mm^2)	67.6	76	58.5
% Elongation	3.0	7	4.0
Stress-Rupture at 1063K and 21.1 Kg/mm^2 following isostatic pressing at 1486K and 10.56 Kg/mm^2	58.6	60	----

(b) Tensile Properties of Machine Cast Cobalt Base Haynes Alloy 31 (From Reference 10)

Tensile Specimen	Temp (K)	Y.S. (Kg/mm^2)	UTS (Kg/mm^2)	El (%)	R.A. (%)
1	R.T.	55.4	72.2	7.2	4.9
2	R.T.	62.2	84	5.0	5.0
Goal	R.T.	35.2	58.5	4.0	7.0
3	1061	28.9	38.4	6.0	5.0
4	1061	26.8	37.6	6.8	6.4
Goal	1061	16.9	40.9	8.0	6.0

(c) Stress-Rupture Properties of Machine Cast Cobalt Base Haynes Alloy 31 Tested At 1061K/21.1 Kg/mm^2 (From Reference 10)

S/R Specimen	Condition	Rupture Life (Hrs)
1	As-Cast	4.7
2	As-Cast	8.5
3	As-Cast + HIP*	28.7
4	As-Cast + HIP*	35.7
5	As-Cast + HIP*	42.1
Goal		30.0

*1486K/10.6Kg/mm^2/4 hours

TABLE II

Tensile Properties of Heat Treated Commercial 6061 Aluminum Alloy Flanged Cup and Cylindrical Parts. Note That Thixoforgings Were Made By Reheating of Previously Rheocast Ingots.

Material	Ultimate Tensile Strength, Kg/mm^2	0.2% Offset Yield Strength, Kg/mm^2	%Elong.
As-Rheocast Ingot, T-4	21.5	17.1	4
Thixoforged T-4	23.8	16.6	12.8
Thixoforged T-6	36	-	9.0
Squeeze Cast No Pressure T-6	32	-	5.1
Squeeze Cast $\sim 10^8$Pa pressure T-6	36	-	14.1
Wrought Alloy from Ref. (12) T-4	24.7	14.8	22
Wrought Alloy from Ref. (12) T-6	31.7	28.2	12

TABLE III

MECHANICAL PROPERTIES OF THIXOFORGED AND SQUEEZE CAST COMMERICAL 2024 ALUMINUM ALLOY (Heat Treated to T-6 Condition)

	Ultimate Tensile Strength, Kg/mm^2	0.2% offset Yield Strength Kg/mm^2	% Elongation
THIXOFORGED			
1	45.1	36.1	11.0
2	47.3	34.3	10.8
3	47.5	35.2	12.3
4	46.8	35.3	11.2
5	43.4	31.8	11.2
6	47.4	35.6	11.3
7	47.3	34.9	10.3
8	46.7	34.3	11.3
Average	46.4 (∿65.9Ksi)	34.7 (∿49.3Ksi)	11.2
SQUEEZE CAST			
1	49.2	36.9	15.6
2	47.4	36.4	14.9
3	48.2	36.8	15.6
4	47.4	36.7	12.4
5	50.2	36.2	8.5
6	47.3	36.8	15.3
7	48.3	35.3	13.7
8	48.9	36.2	11.8
9	47.7	34.2	14.0
10	48.3	36.2	12.8
Average	48.3 (∿68.6Ksi)	36.2 (∿51.4Ksi)	13.4
WROUGHT ALLOY			
in T-6 condition (from Ref. (12))	48.5 (∿69Ksi)	∿40(57Ksi)	10

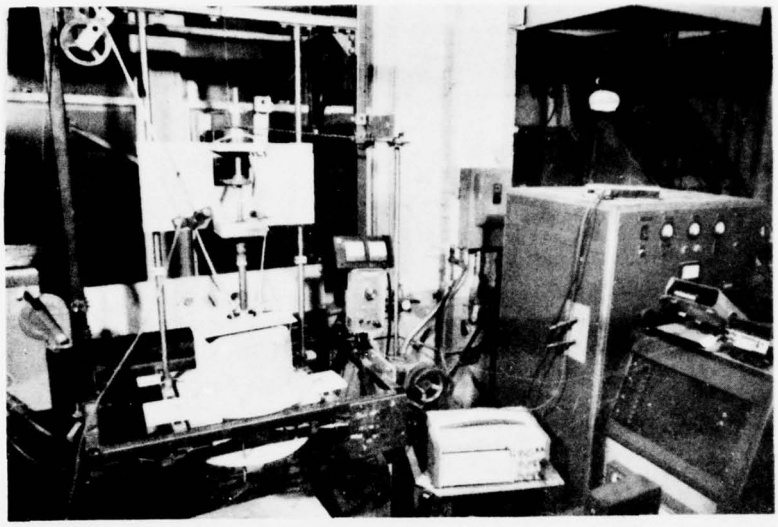

(a)

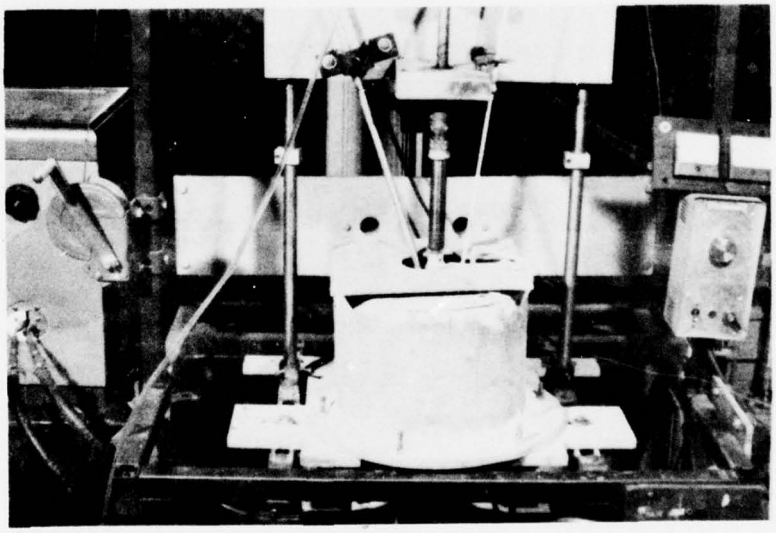

(b)

Figure 1. Photographs of the continuous slurry producer; (a) shows an overall view of the apparatus with some of the associated power supplies and control systems; (b) shows the top chamber of the apparatus into which a solid rod of an alloy is fed continuously.

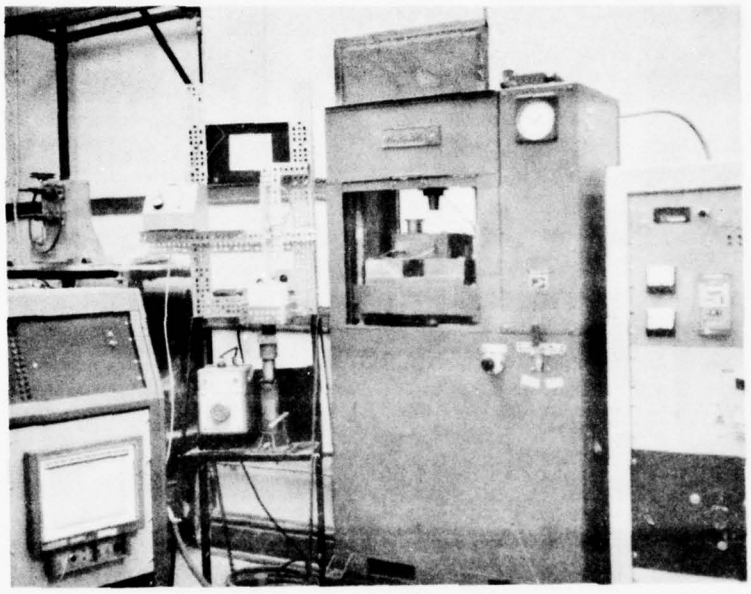

(a)

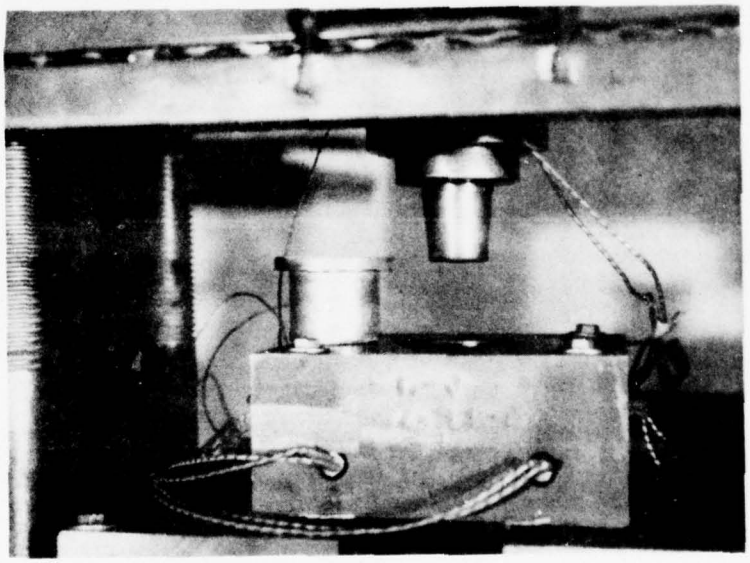

(b)

Figure 2. Photograph of laboratory Thixoforging apparatus; (a) shows an overall view of the apparatus including the resistance reheat furnace, penetrometer, hydraulic press and temperature controllers; (b) shows the two die halves and a Thixoforged aluminum alloy cup shaped part.

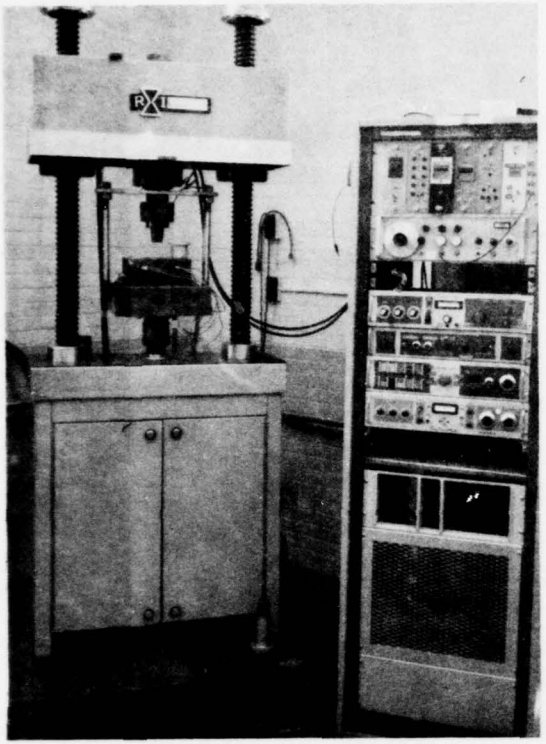

(a)

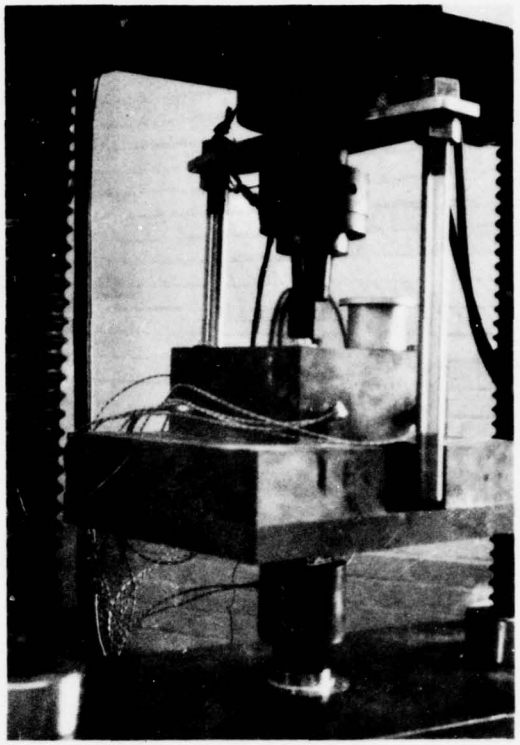

(b)

Figure 3. Photographs of the MTS system used in the laboratory Thixoforging apparatus; (a) shows the MTS hydraulic power supply with its associated load-stroke control system; (b) shows a close-up of the die assembly and a Thixoforged aluminum alloy cup shaped part.

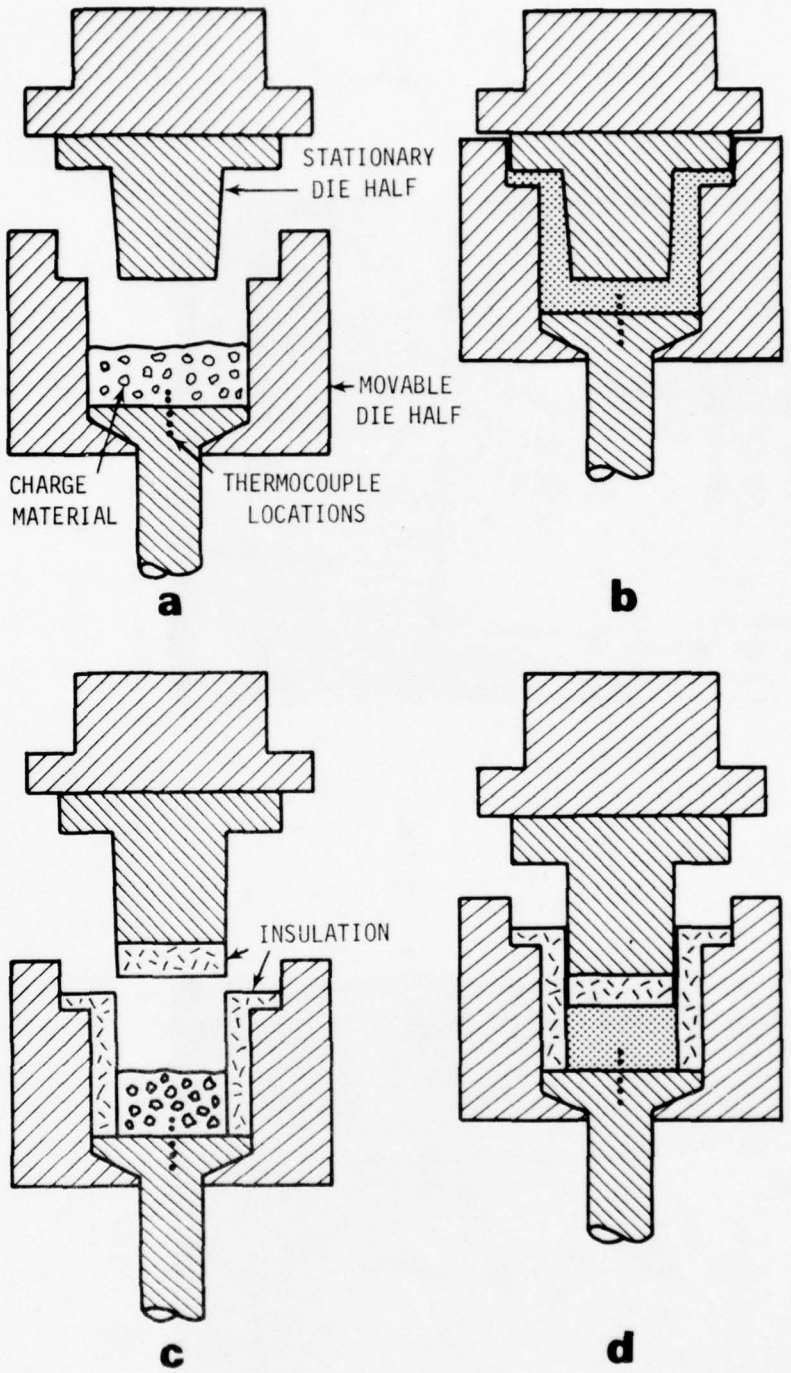

Figure 4. Schematic illustration of the dies used in the laboratory Thixoforging apparatuses; (a) and (b) represent the cup shaped part; (c) and (d) represent the cylindrical parts unidirectionally solidified by heat extraction from the bottom.

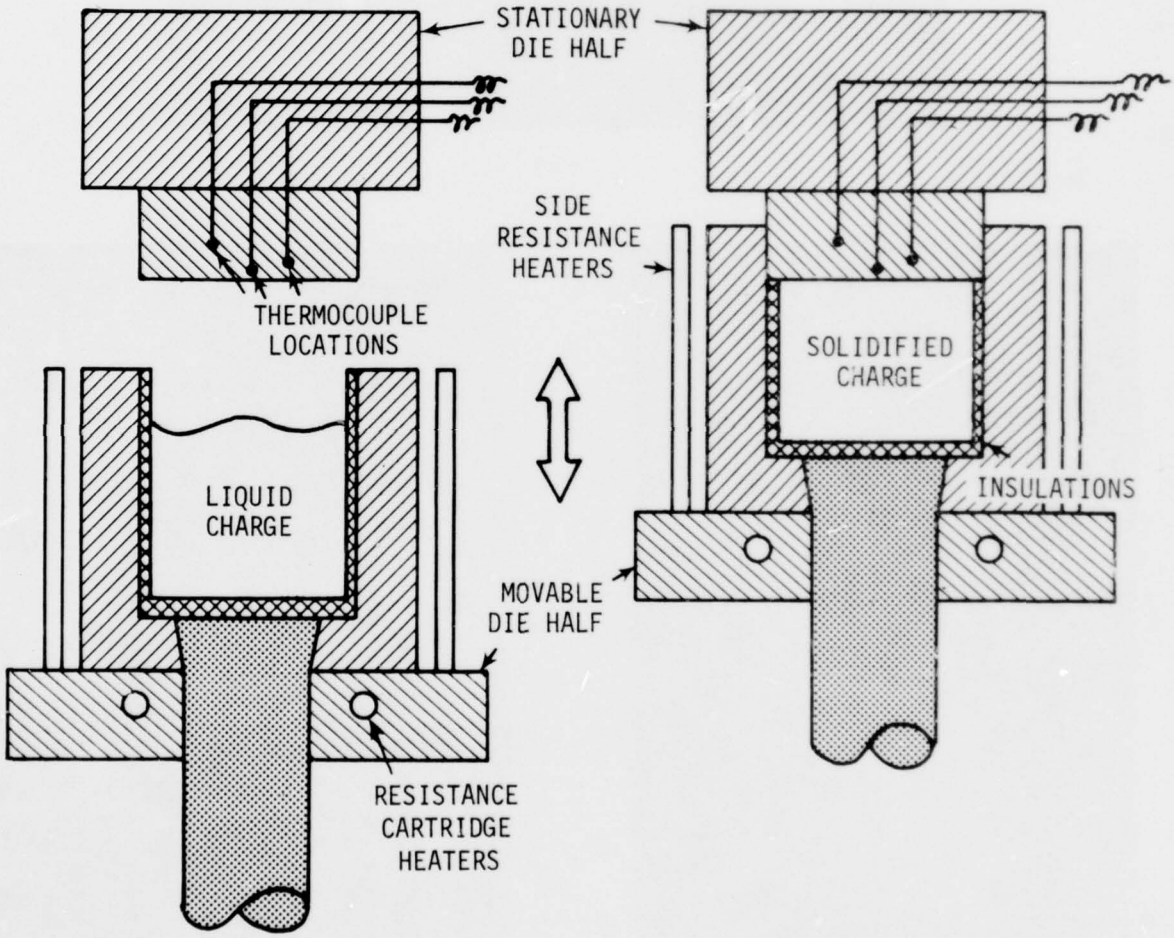

Figure 5. Schematic illustration of the dies used in the recent die thermal behavior studies. Thermocouples are located in the cold top die half which extracts heat from the cylindrical specimen simultaneously with pressurization.

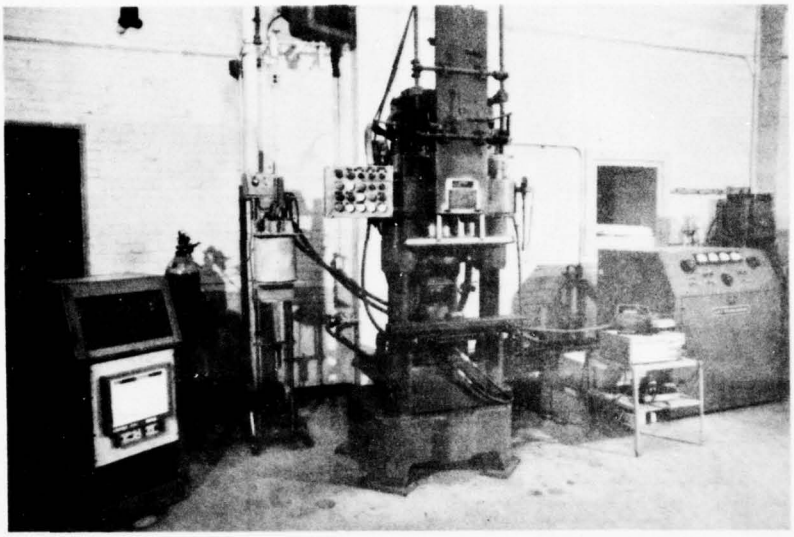

(a)

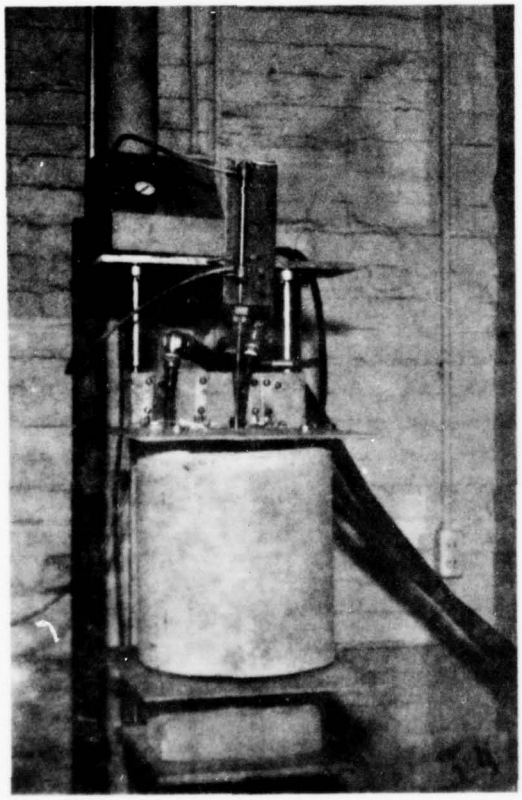

(b)

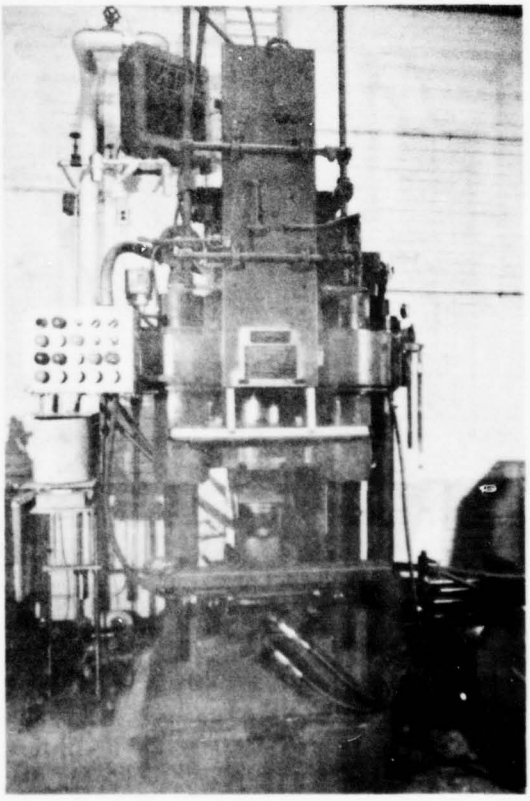

(c)

Figure 6. Photographs of the pilot plant Thixoforging system; (a) shows an overall view of the apparatus including the induction powered reheat furnace and the associated power supply; (b) shows the reheat furnace with the controlled pressure penetrometer located on top of it; (c) shows a close-up of the 200 ton press and its automatically controlled plexiglass shield which moves down to protect the operator.

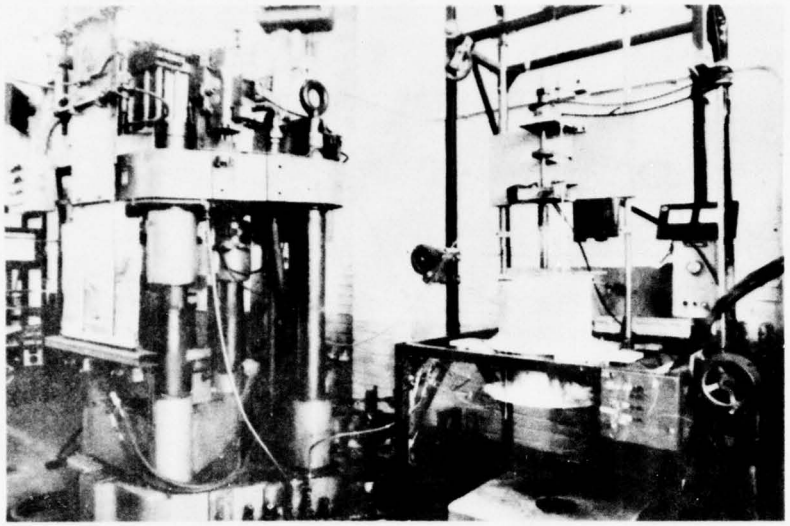

(a)

(b)

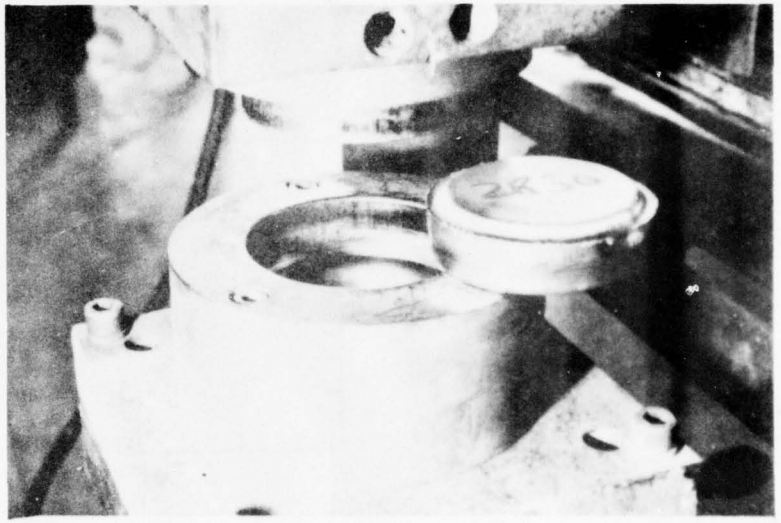

(c)

Figure 7. Photographs of the pilot plant forging press, continuous Rheocasting apparatus, ladles used for charge transfer, the dies and parts produced.

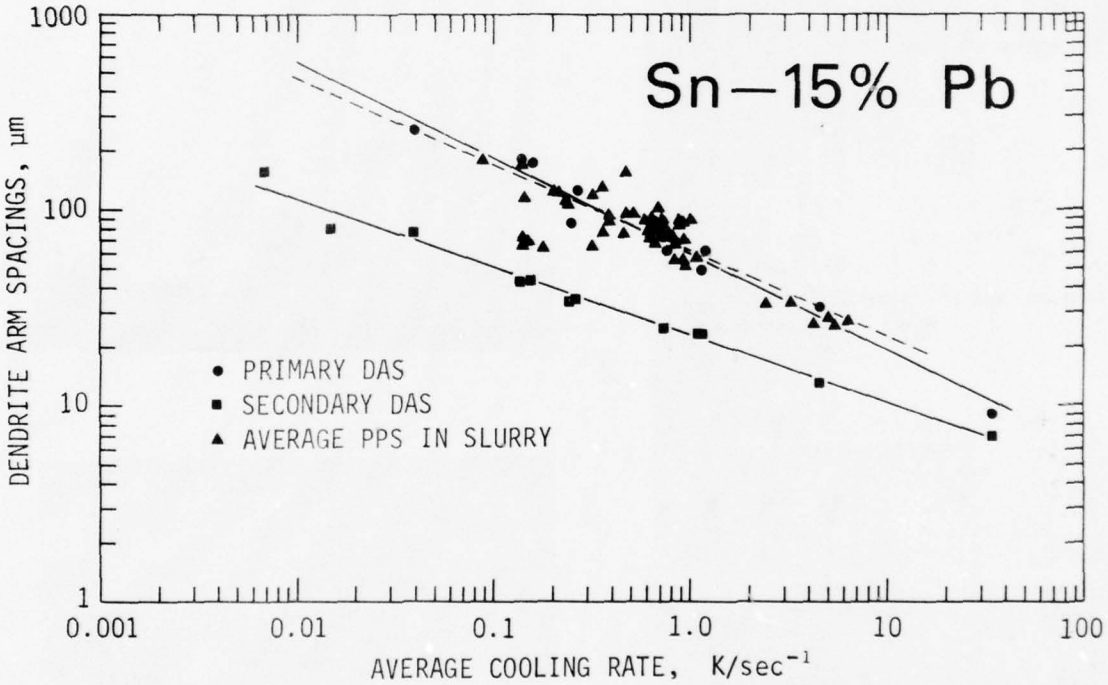

Figure 8. Variation of dendrite arm spacings, DAS, in conventionally cast, and variation of primary solid particle size, average PPS, in continuously produced slurry of Sn-15% Pb alloy with cooling rate during solidification (from Reference 5).

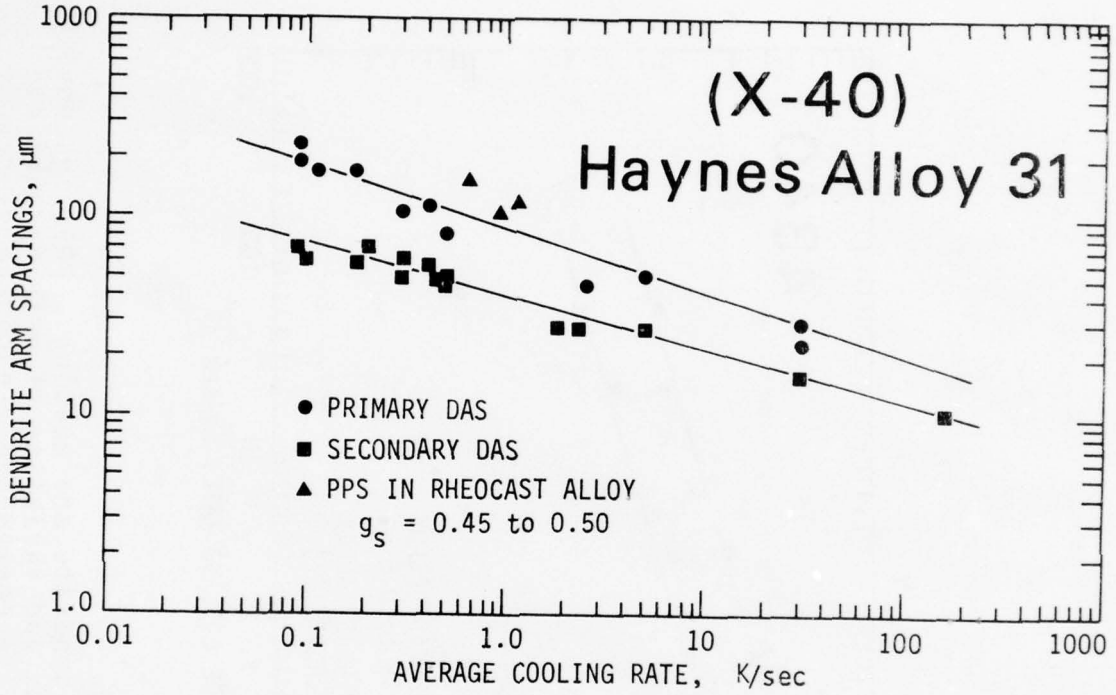

Figure 9. Variation of dendrite arm spacings, DAS, in conventionally cast, and variation of primary solid particle size, p.p.s, in continuously produced slurry of cobalt base Haynes alloy 31 (alternate designation X-40) with average cooling rate during solidification.

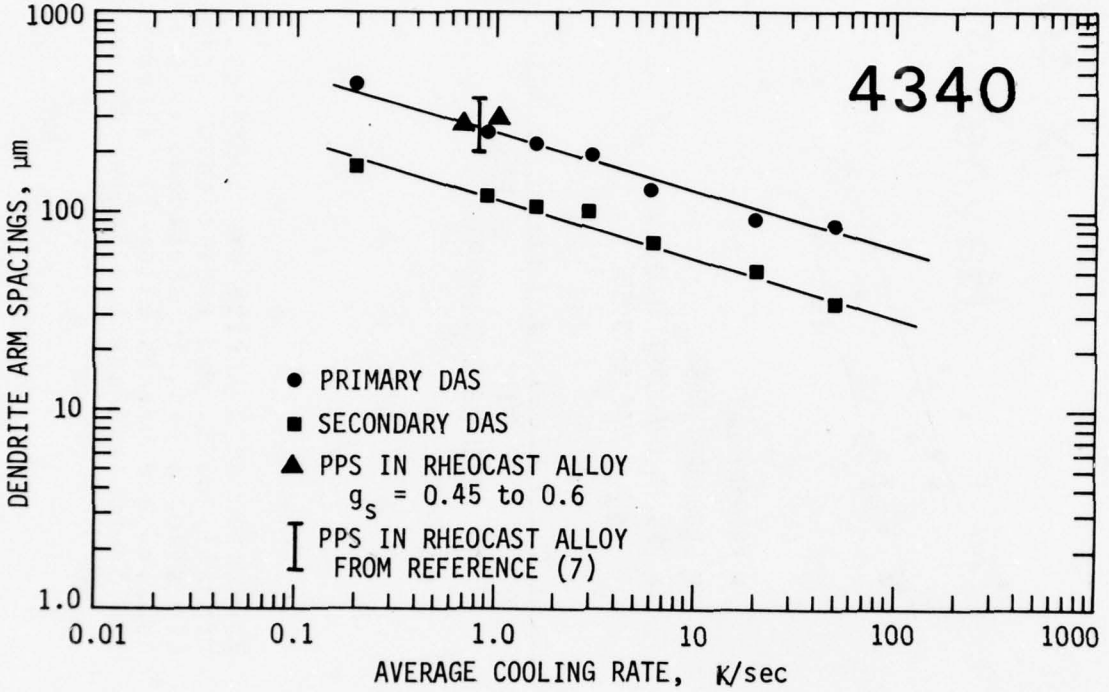

Figure 10. Variation of dendrite arm spacings, DAS, in conventionally cast, and variation of primary particle size, p.p.s., in continuously produced slurry of AISI 4340 low alloy steel with average cooling rate during solidification.

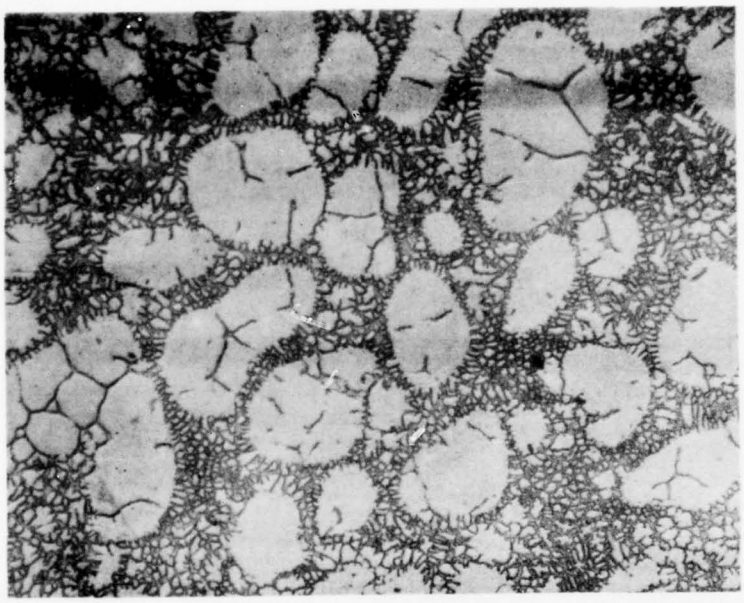

a

b

Figure 11. Microstructure of Rheocast cobalt-base Haynes alloy 31; (a) water quenched specimen showning spheroidal primary solid particles delineated by the rapidly solidified remaining liquid in the slurry; (b) ingot microstructure. Magnification 50X.

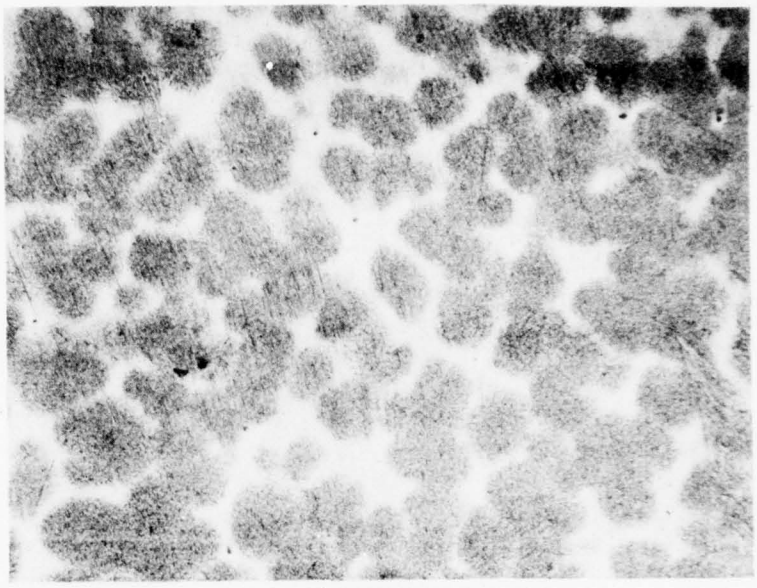

a

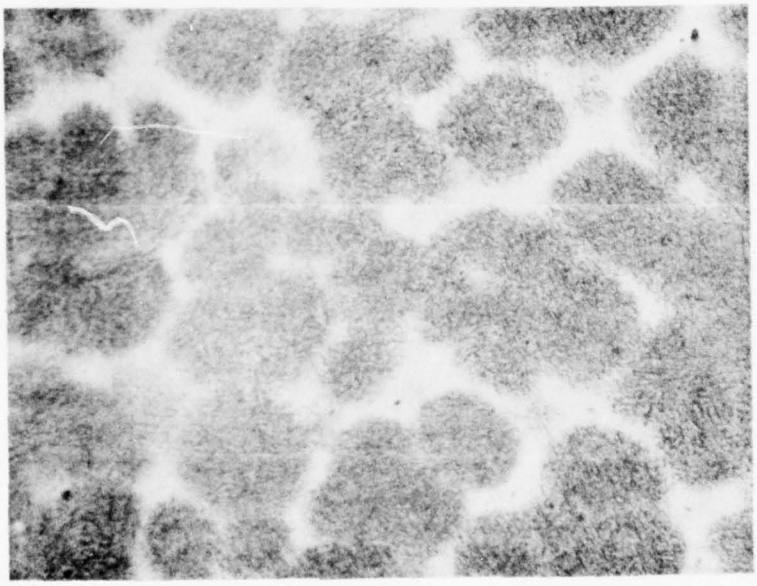

b

Figure 12. Microstructure of Rheocast 4340 low alloy steel; (a) magnification 50X, (b) magnification 100X.

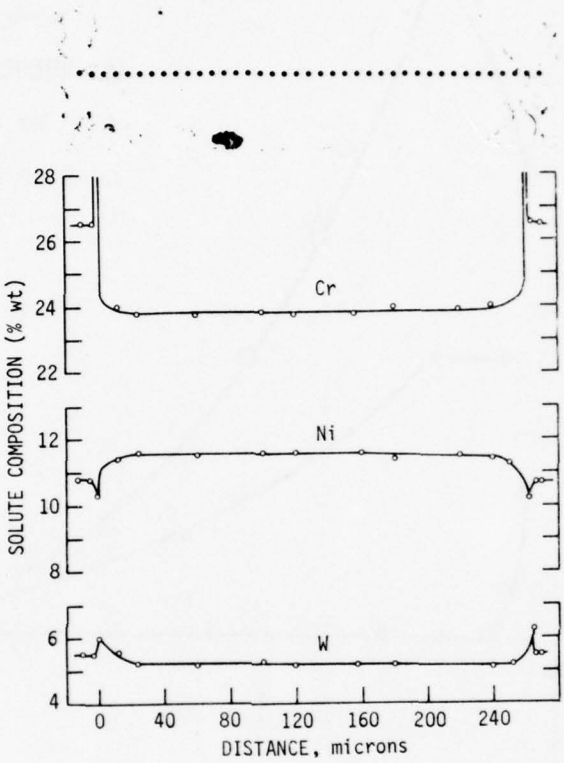

Figure 13. Composite figure showing the microprobe traces and photograph of the microstructure of Rheocast cobalt-base Haynes alloy 31. Solute distribution is along dotted path shown in the photograph. Both the graph and the photograph have the same scale in the horizontal direction.

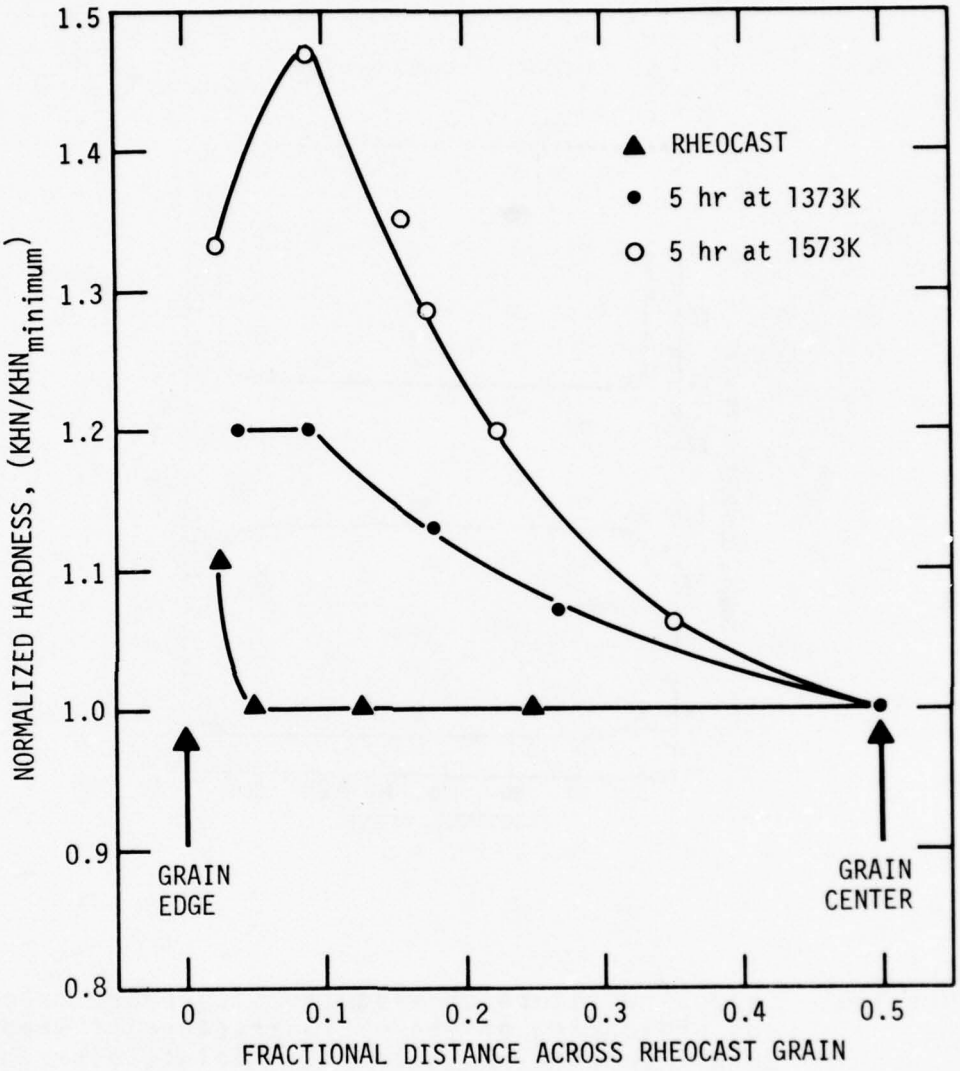

Figure 14. Measured variation of microhardness, normalized as the ratio of Knoop hardness number at a given location against the minimum value, across the Rheocast grain of cobalt-base Haynes alloy 31 in the as-Rheocast and homogenized, heat treated, conditions.

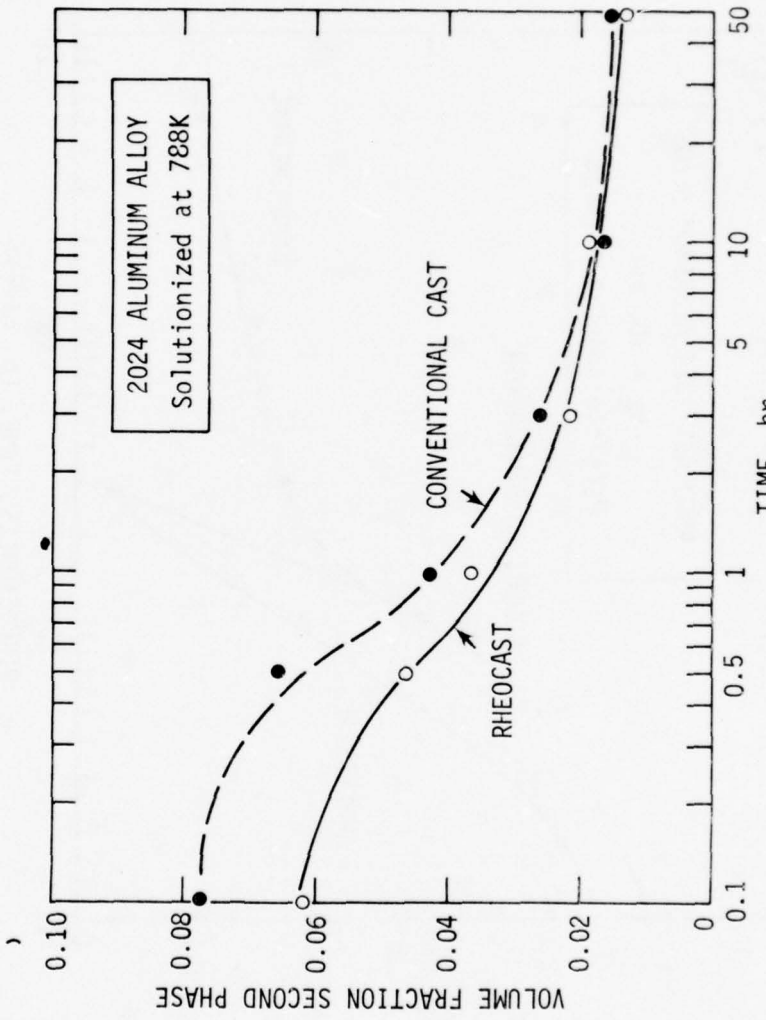

Figure 15. Plot of experimentally measured volume fraction of second phase as a function of solution time at 788K for conventional cast and Rheocast 2024 aluminum base alloy.

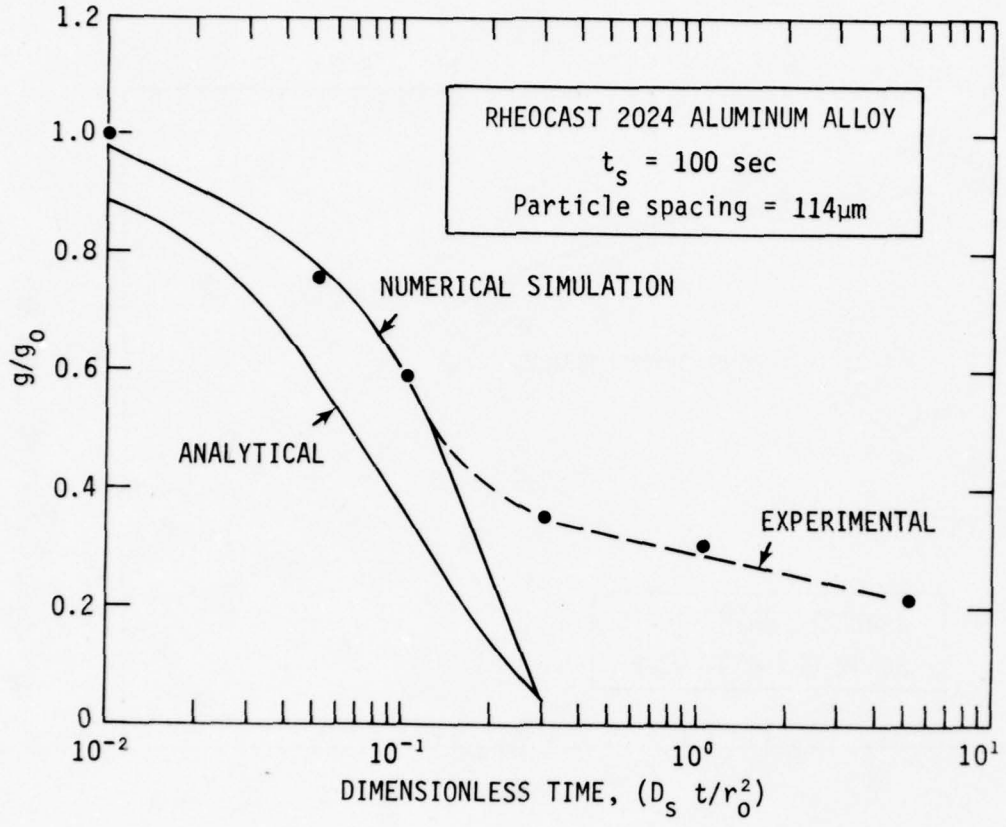

Figure 16. Plot of normalized second phase content g/g_o; as a function of dimensionless time, $D_s\ t/r_o^2$, for a Rheocast commercial aluminum alloy. The plots were determined by analytical and numerical solution of the solutionization model employing a spherical growth morphology.

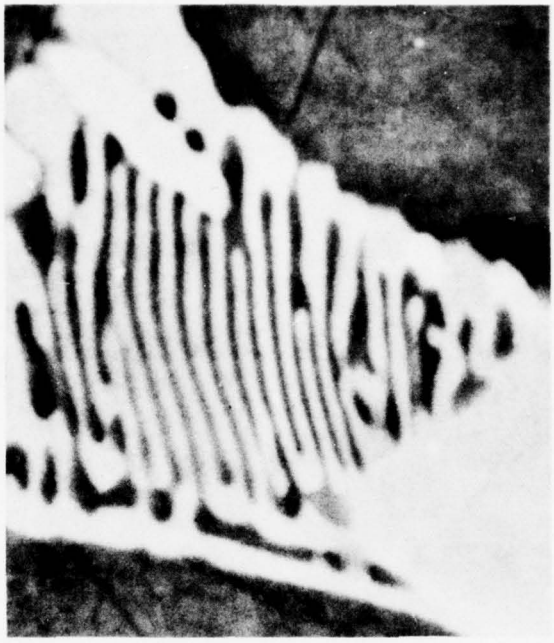

(a)

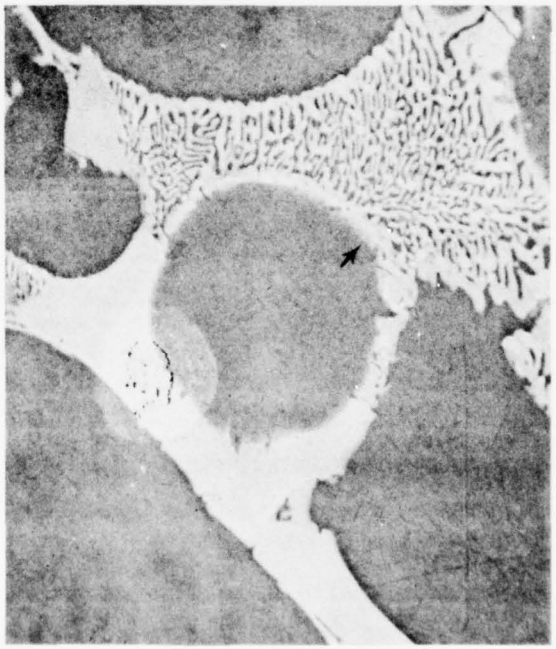

(b)

Figure 17 Secondary Electron Images of the eutectic phases in the as-Rheocast commerical 2024 aluminum alloy. (a) and (b) show the structure of α + $CuAl_2$ at 5000X and α + $CuAl_2$ + $CuMgAl_2$ at 800X, respectively.

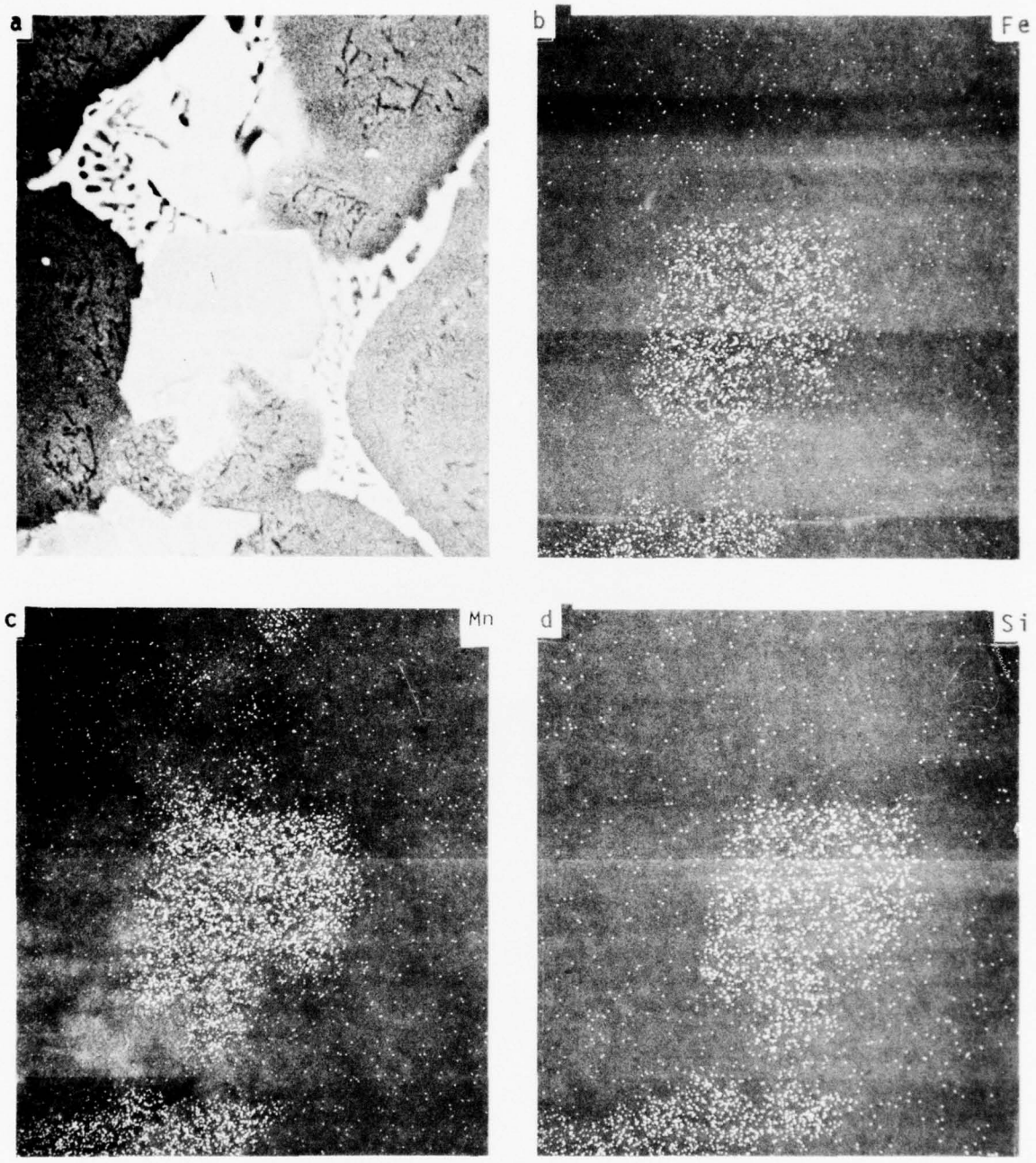

Figure 18 Secondary Electron Image and elemental x-ray maps of two α(Al-Fe-Mn-Si) particles in the as-Rheocast commercial 2024 aluminum alloy at 1000X.

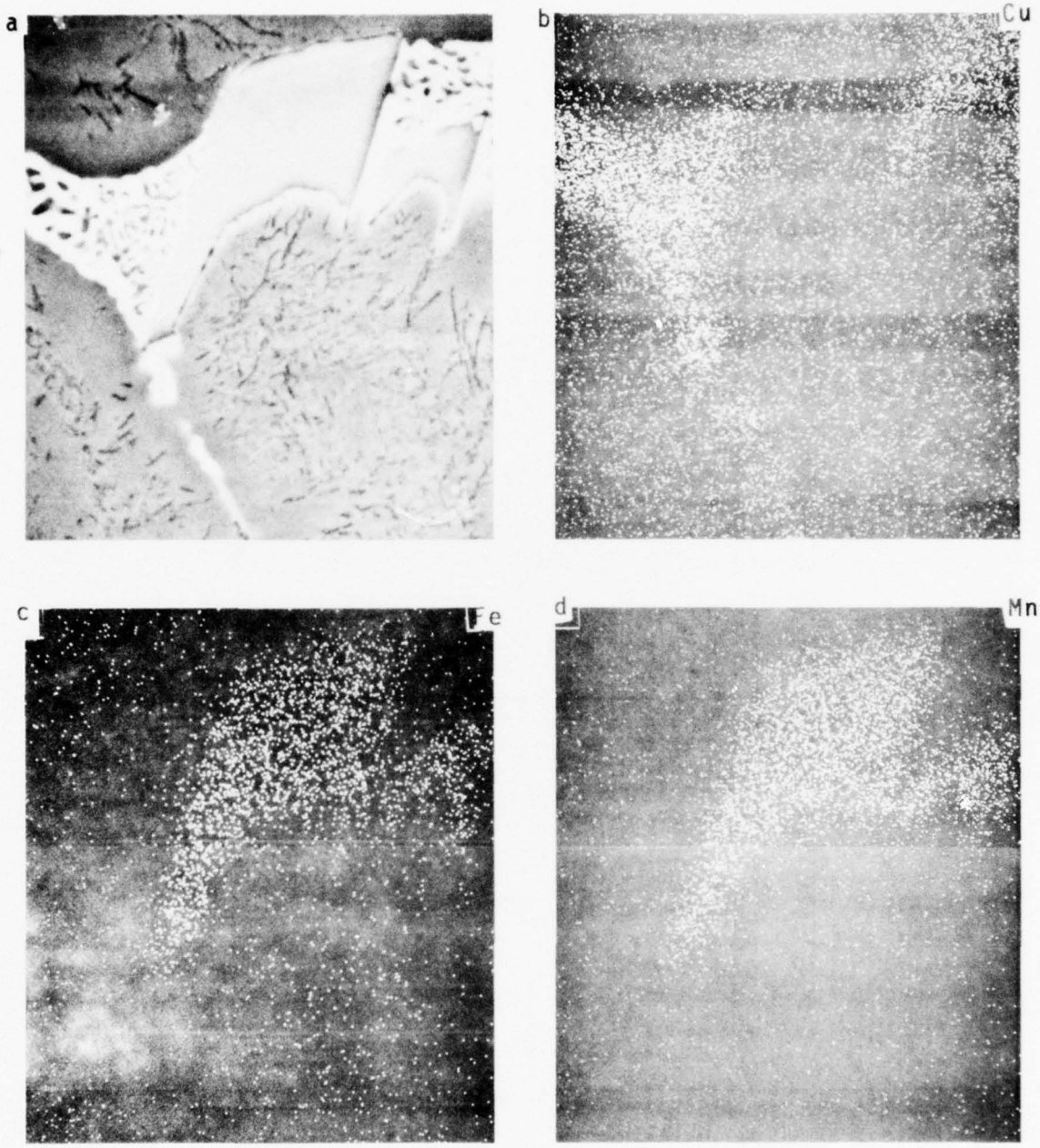

Figure 19 Secondary Electron Image and elemental x-ray maps of particles of $(Cu\text{-}Fe\text{-}Mn)Al_6$ in the as-Rheocast 2024 commercial aluminum alloy at 1000X.

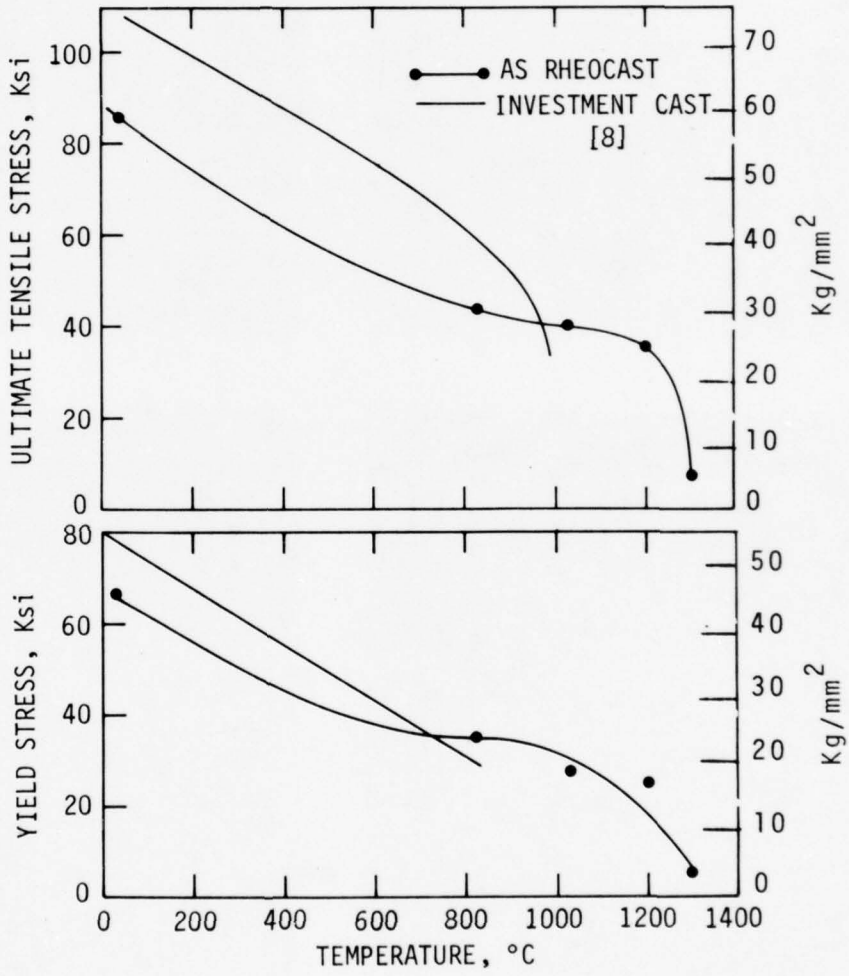

Figure 20. Yield and ultimate tensile stress versus temperature in rapid strain rate tensile test, Gleeble test. As-Rheocast cobalt-base Haynes alloy 301.

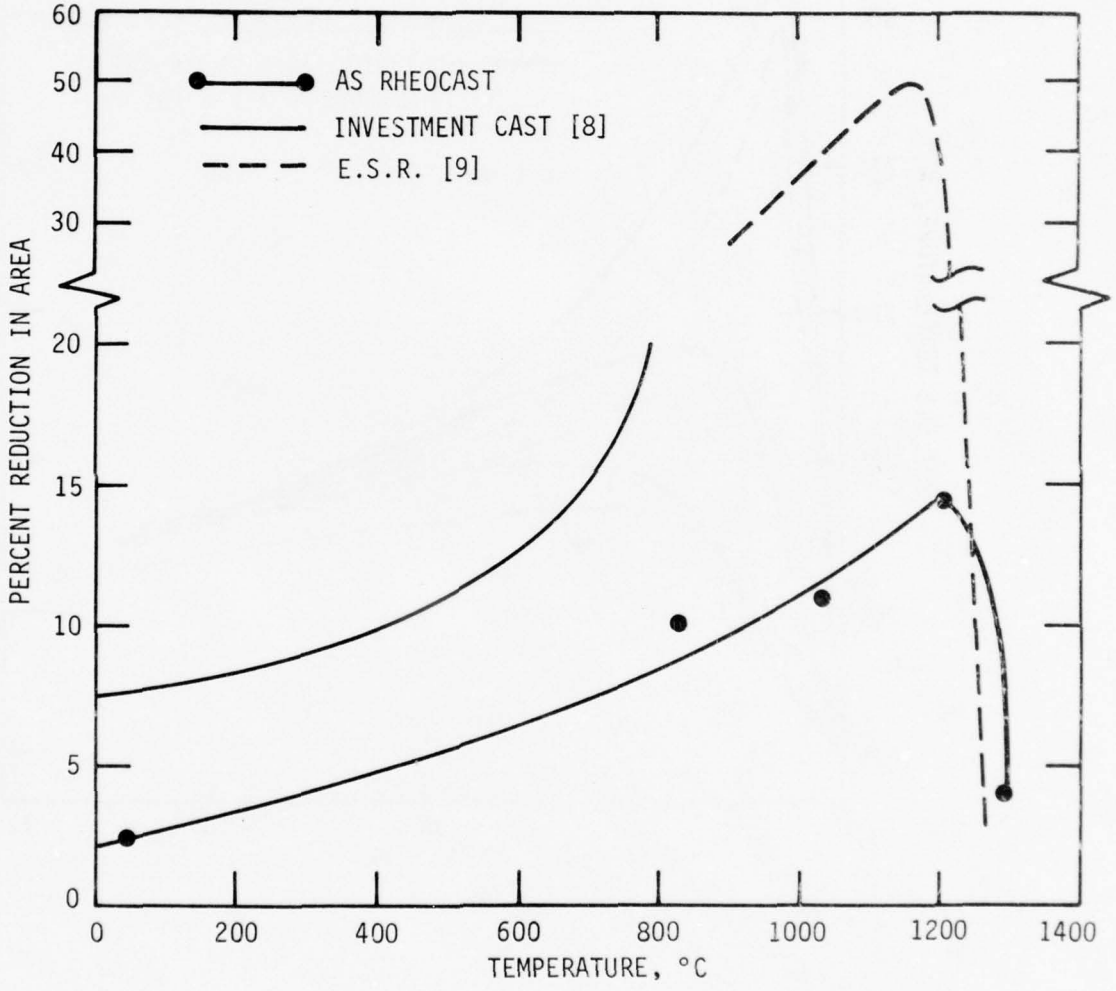

Figure 21. Reduction in area versus temperature in rapid strain rate tensile test, Gleeble test. As-Rheocast cobalt-base Haynes alloy 31.

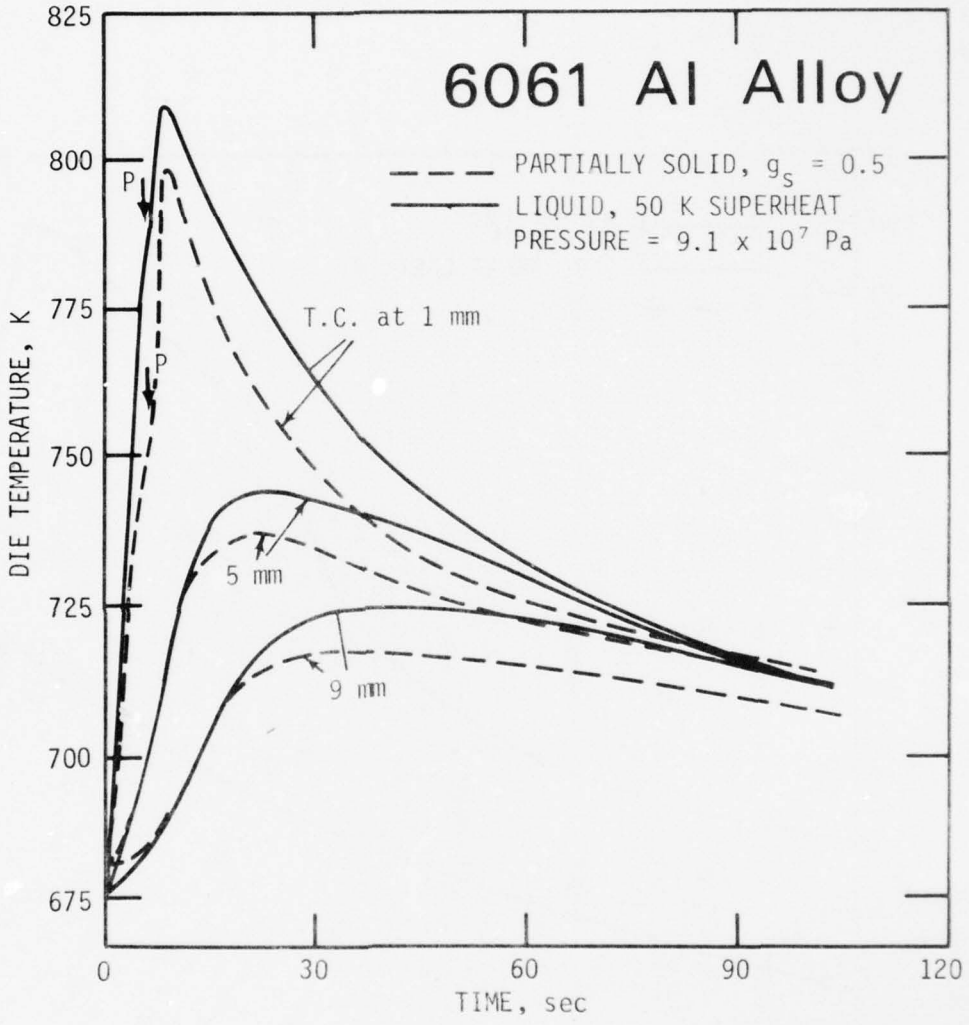

Figure 22. Die thermal response -- comparison between a superheated liquid and a partially solid initial charge (3).

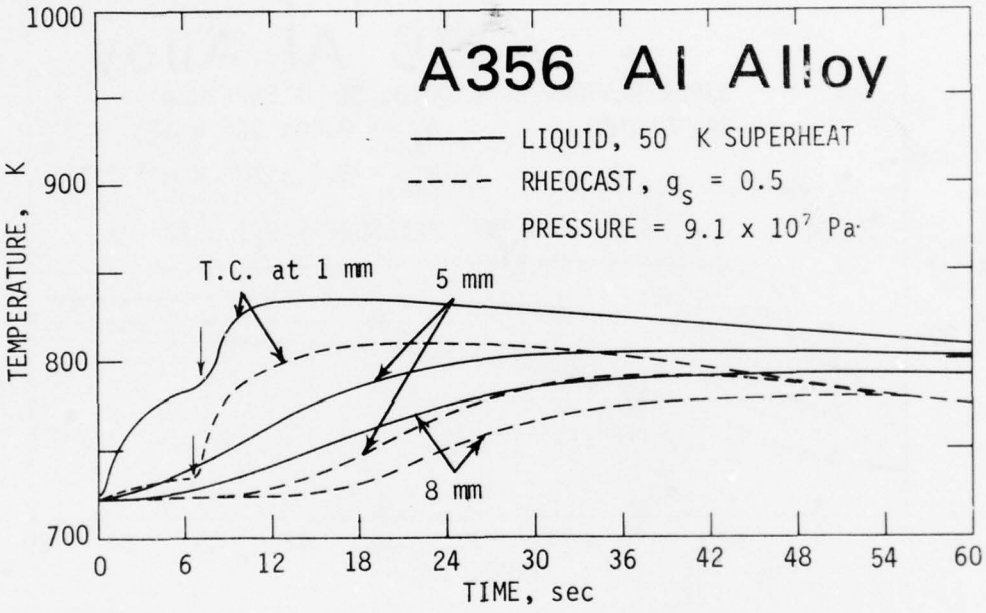

Figure 23. Die thermal response -- comparison between a superheated liquid and a partially solid initial charge (3).

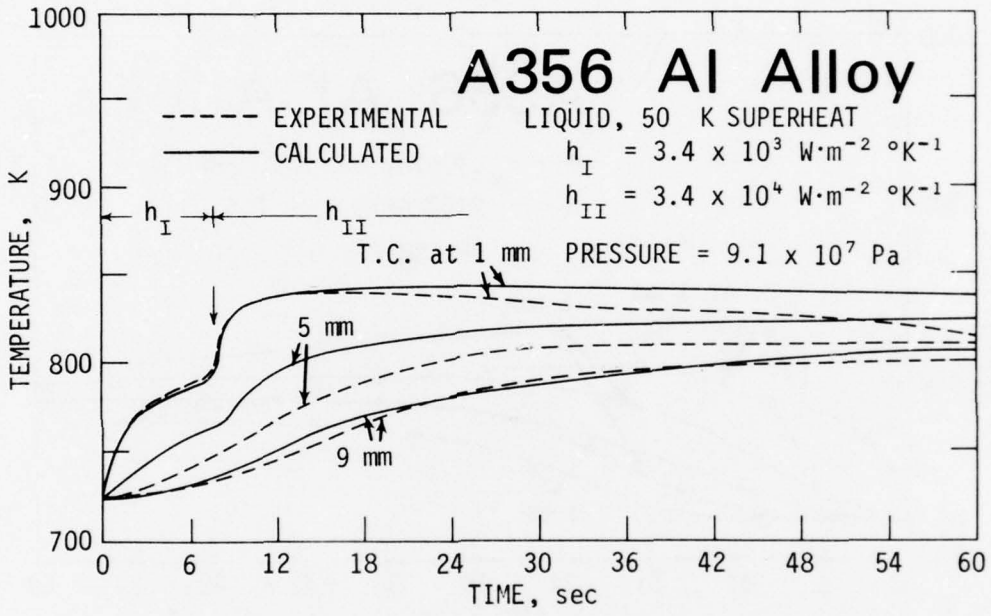

Figure 24. Die thermal response -- comparison between measured and calculated temperature profiles (3).

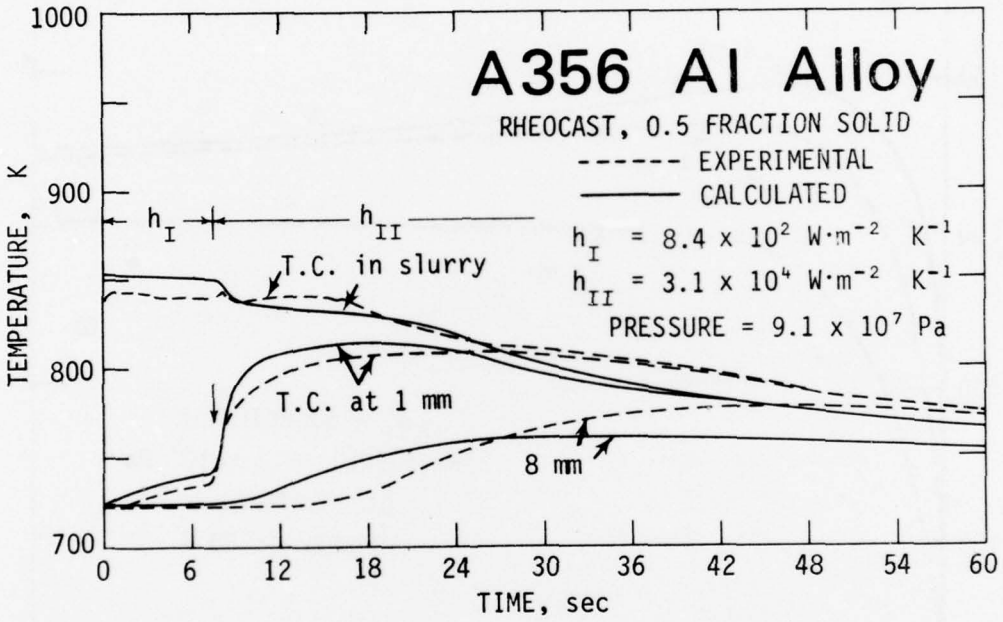

Figure 25. Composite of die and forging thermal responses -- comparison between measured and calculated temperature profiles (3).

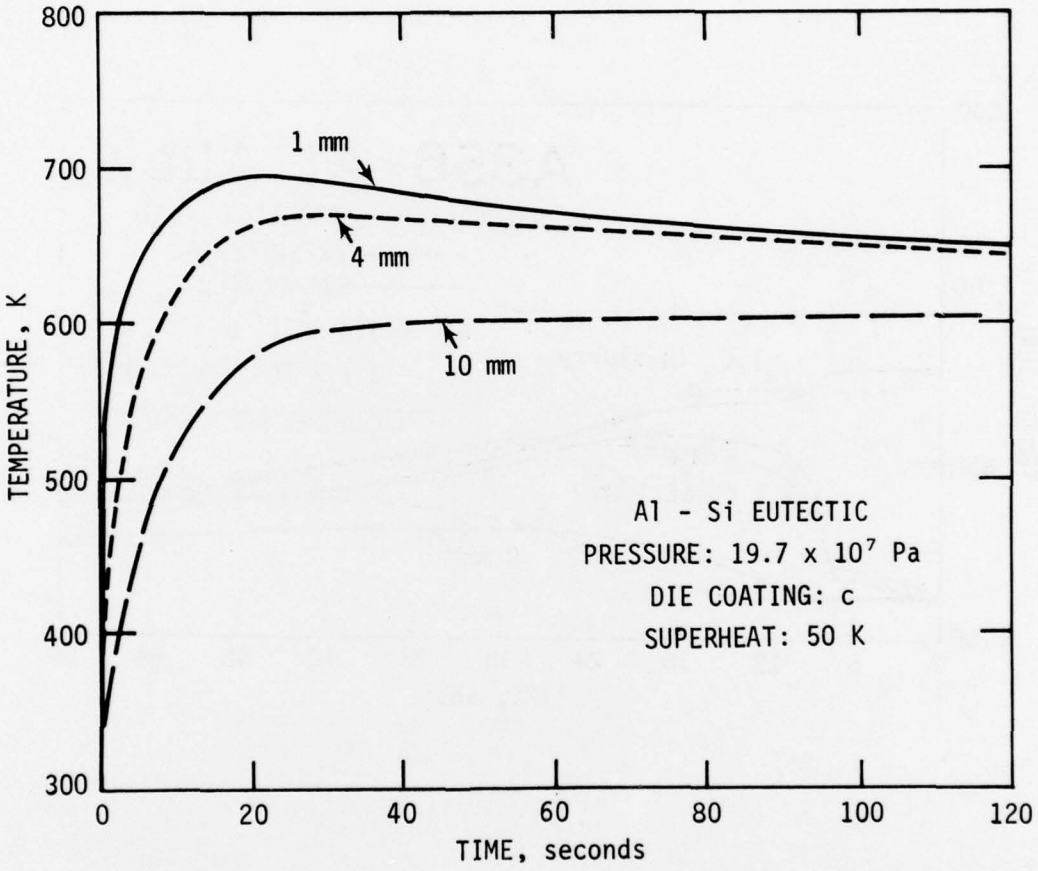

Figure 26. Die thermal response at a high applied pressure of 19.7 x 10^7pa and a 0.05mm thick die coating of graphite powders in isopropyl alcohol.

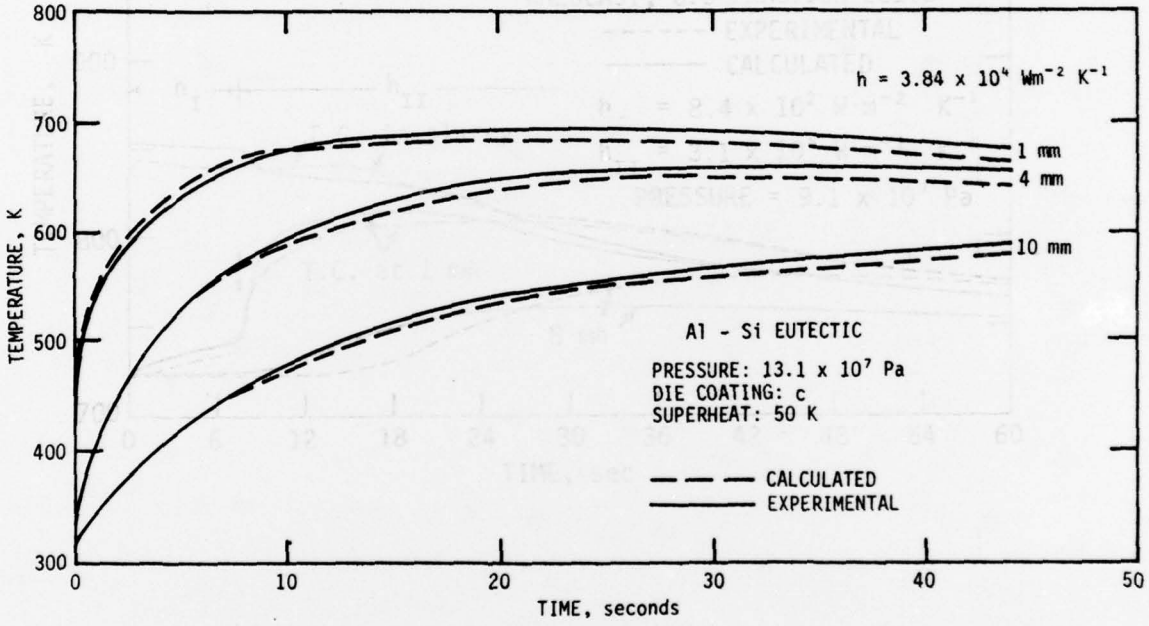

Figure 27. Die thermal response - comparison between computer simulation and actual measured die temperatures.

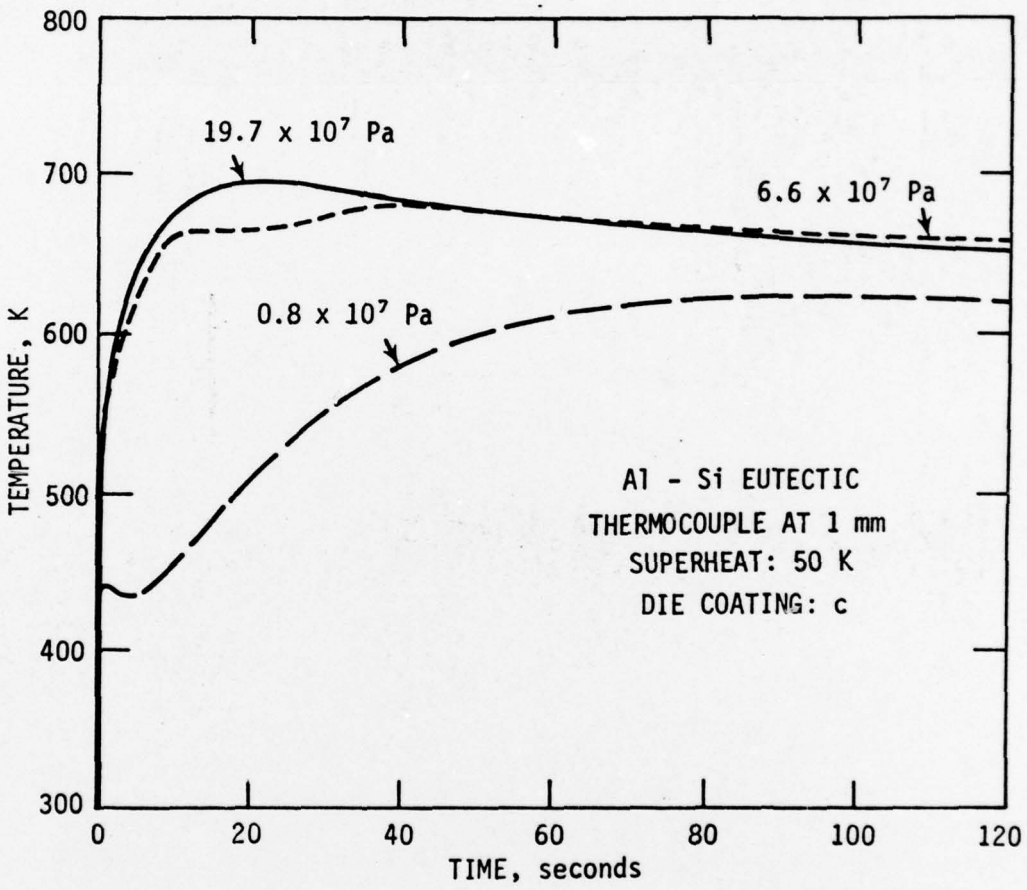

Figure 28. Die thermal response - effect of applied pressure on recorded temperature at 1mm from the metal-die interface.

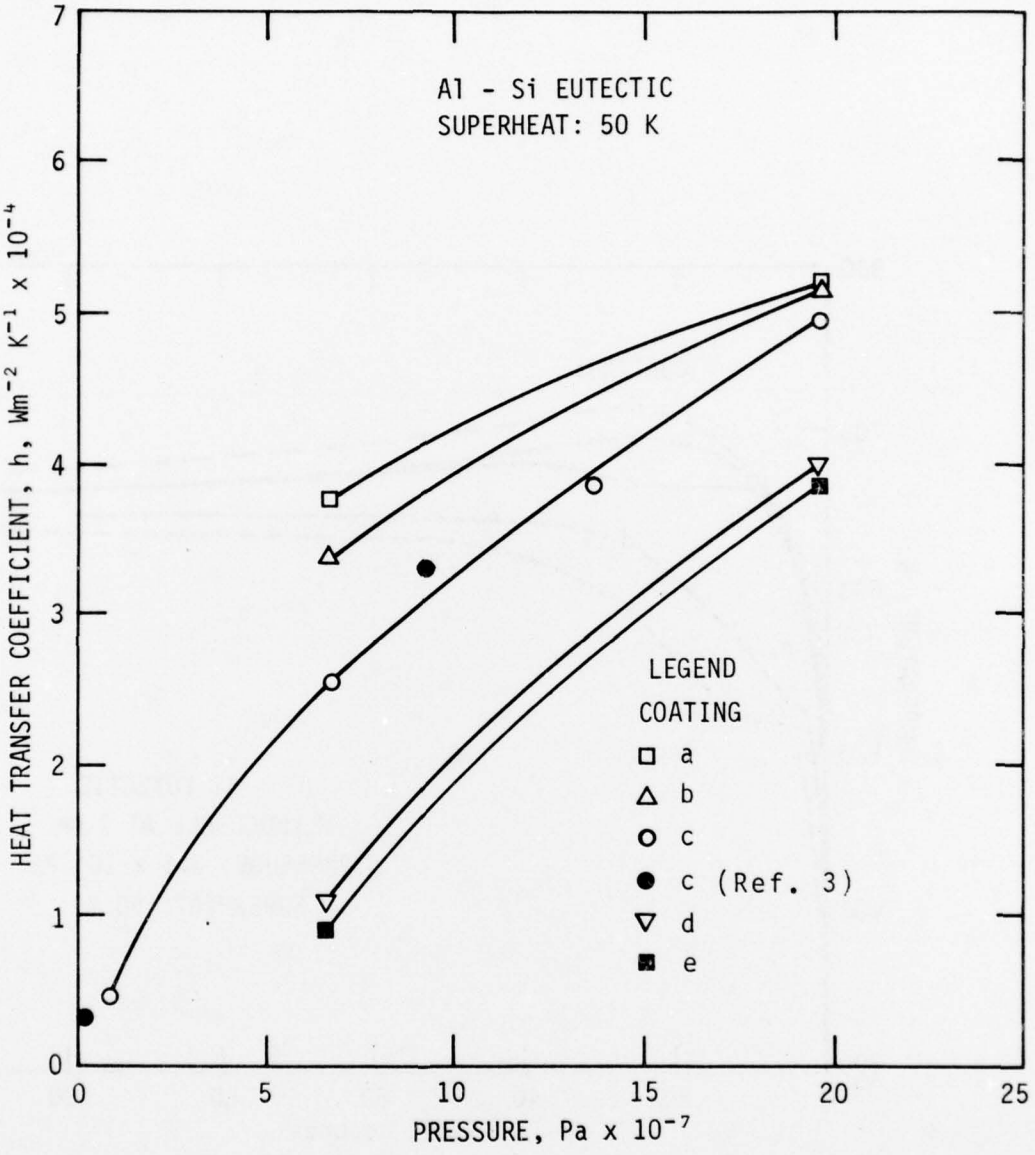

Figure 29. Effect of applied pressure and die coating on the heat transfer coefficient at the metal-die interface.

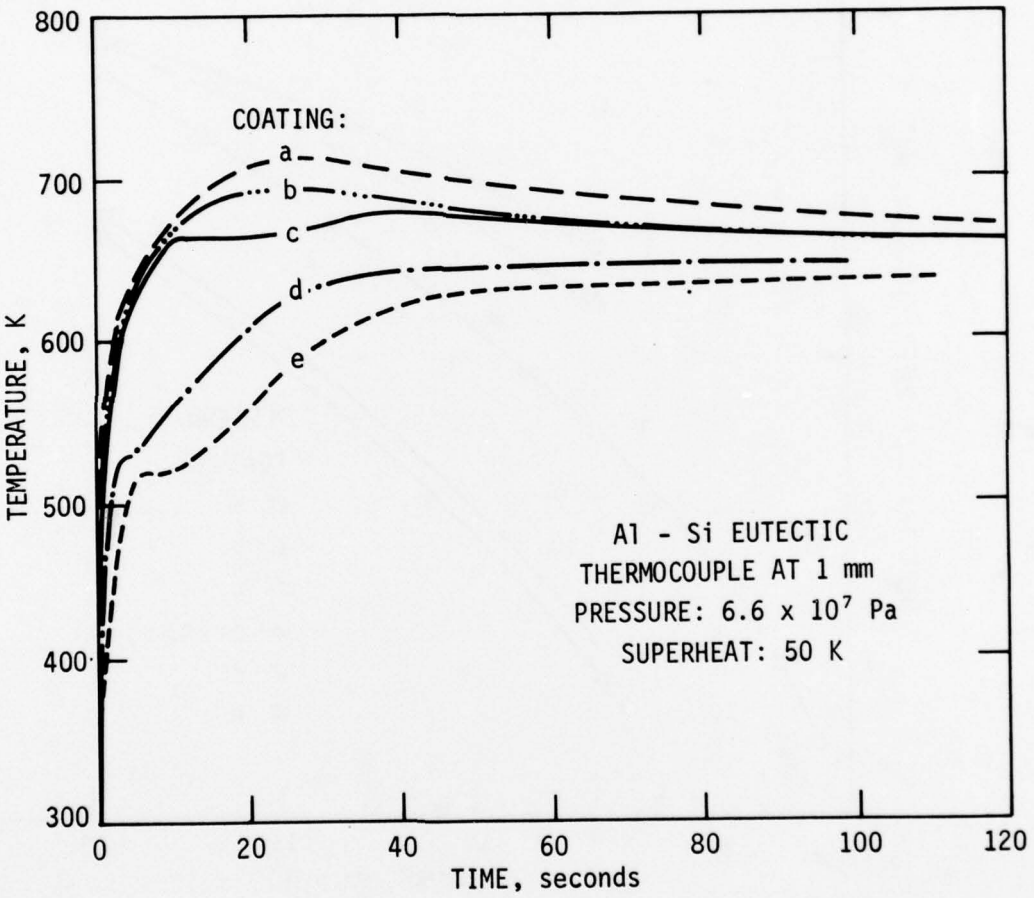

Figure 30. Die thermal response - effect of die coating on recorded die temperatures at 1mm from the metal-die interface.

(a)

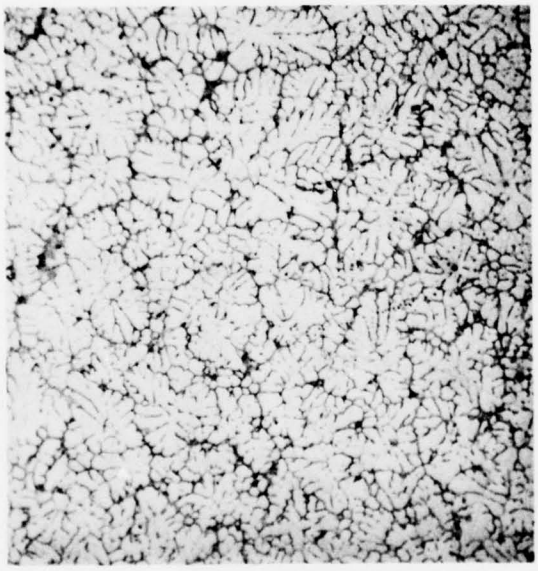

(b)

Figure 31. Microstructures of commercial 6061 aluminum alloy cup shaped parts at 55X magnification. (a) Thixo-forged part - initial volume fraction solid ∿0.65, (b) Part made from a superheated (∿50K) liquid.

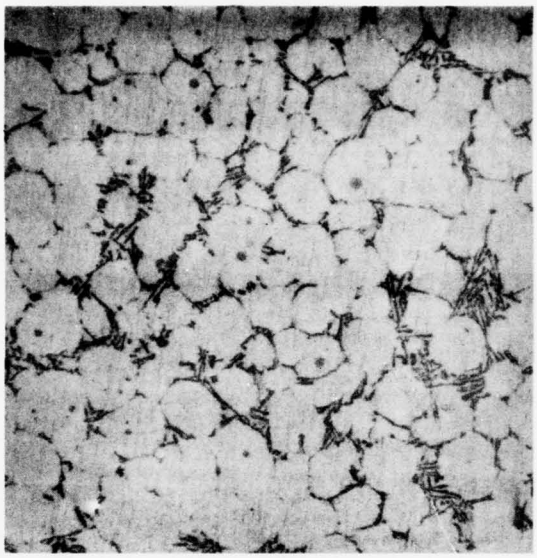

(a)

(b)

Figure 32. Microstructures of commercial A356 aluminum alloy forgings made in the unidirectional die cavity. Magnification 100X. (a) Thixoforged part - initial volume fraction solid ∿ 0.6. (b) Part made from a superheated (∿50K) liquid.

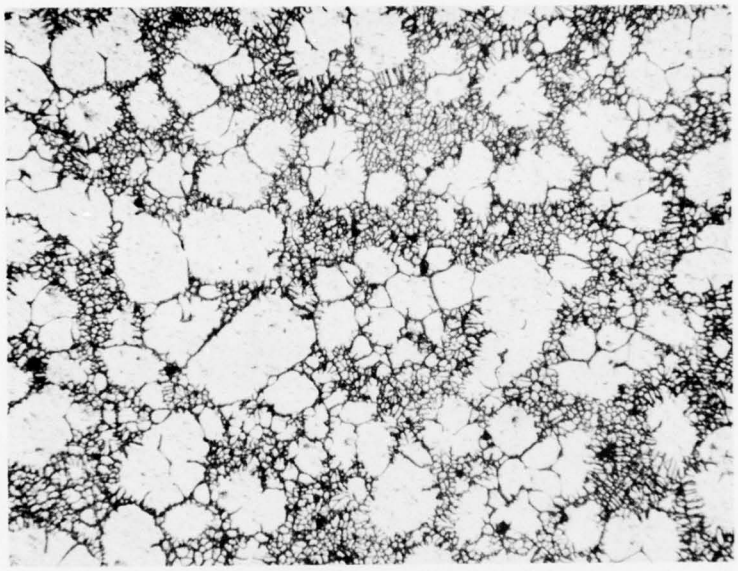

Figure 33. Typical structure of Rheocast and water quenched commercial 2024 aluminum alloy at 70X.

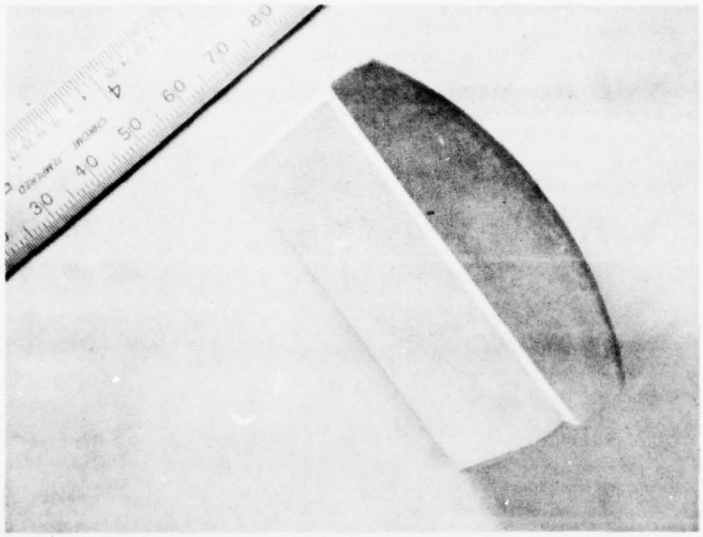

(a)

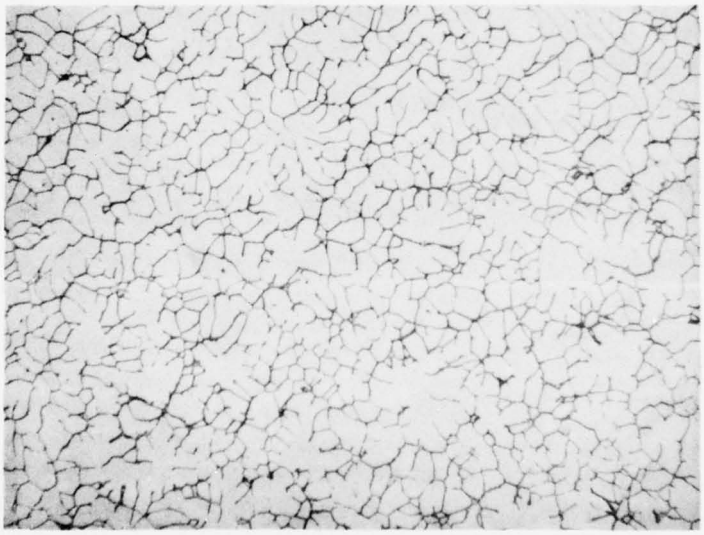

(b)

Figure 34. Cross-sectional views of a Thixoforged commercial 2024 aluminum alloy disc shaped part; (a) shows the microstructure of a section of the part; (b) shows the microstruct + 70X.

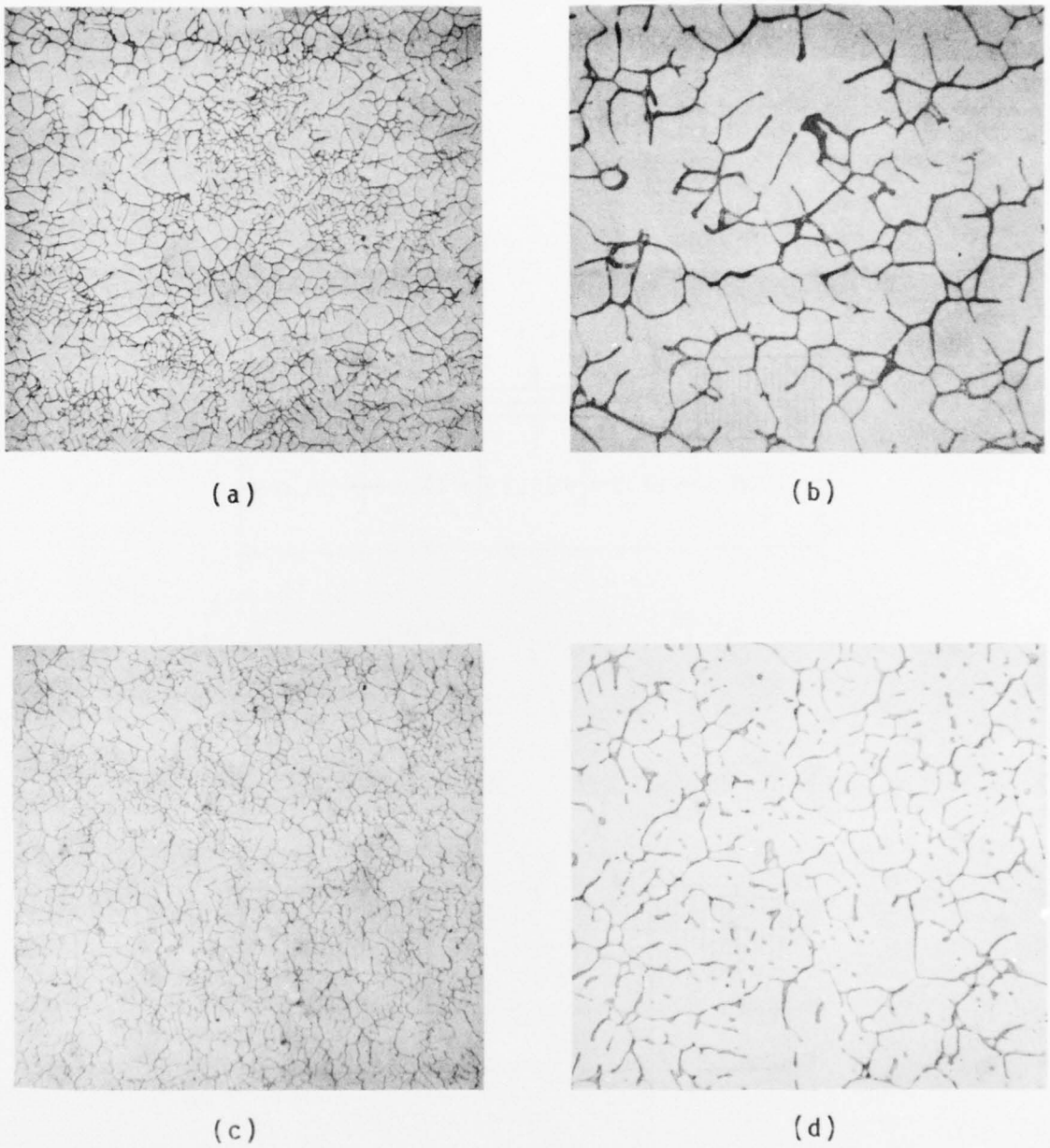

Figure 35. Microstructure of disc shaped parts. (a) and (b) show the microstructure of a Thixoforged part at 70X and 180X, respectively. (c) and (d) show the microstructure of a Squeeze Cast part at 70X and 180X, respectively.

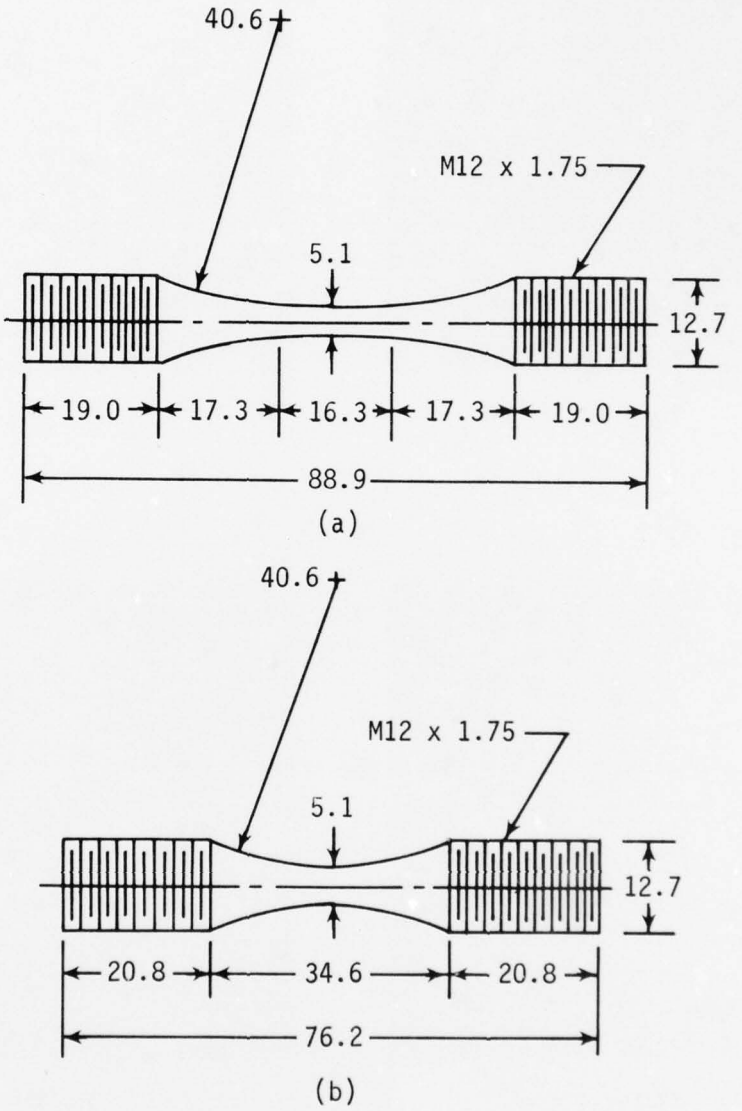

Figure 36. Dimensions (in mm) of the two types of specimens used in the constant stress fatigue tests.

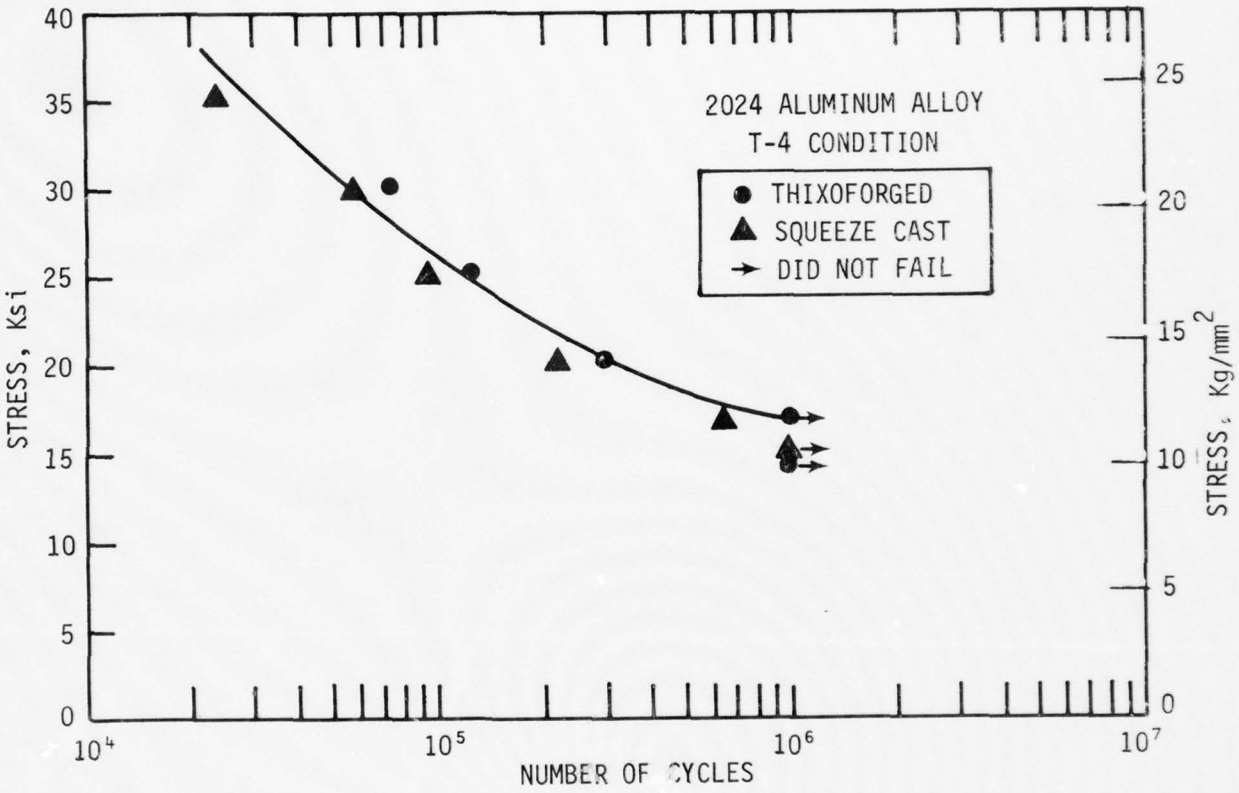

Figure 37. Results of constant stress compression-tension fatigue life tests carried out on Thixoforged and Squeeze Cast commercial 2024 aluminum base alloy disc-shaped parts.